frontiers | Frontiers in Earth Science

TYPE Methods
PUBLISHED 17 April 2025
DOI 10.3389/feart.2025.1523730

OPEN ACCESS

EDITED BY
Randel Tom Cox,
University of Memphis, United States

REVIEWED BY
Merghadi Abdelaziz,
University of Tébessa, Algeria
Matteo Fiorucci,
University of Cassino, Italy

*CORRESPONDENCE
Deborah Maceroni,
deborah.maceroni@isprambiente.it

RECEIVED 06 November 2024
ACCEPTED 06 March 2025
PUBLISHED 17 April 2025

CITATION
Tallini M, Maceroni D, Falcucci E, Galadini F, Gori S, Guerriero V, Spadi M, Moro M and Saroli M (2025) Multi-methodological approach for assessing surface faulting and paleoliquefaction history in central Italy: applicative implications for seismic microzonation studies in the Quaternary L'Aquila basin.
Front. Earth Sci. 13:1523730.
doi: 10.3389/feart.2025.1523730

Multi-methodological approach for assessing surface faulting and paleoliquefaction history in central Italy: applicative implications for seismic microzonation studies in the Quaternary L'Aquila basin

Marco Tallini[1], Deborah Maceroni[2]*, Emanuela Falcucci[3], Fabrizio Galadini[3], Stefano Gori[3], Vincenzo Guerriero[1], Marco Spadi[1], Marco Moro[3] and Michele Saroli[4,3]

[1]Dipartimento di Ingegneria Civile, Edile-Architettura e Ambientale (DICEAA), Università degli Studi dell'Aquila, L'Aquila, Italy, [2]Istituto Superiore per la Protezione e Ricerca Ambientale (ISPRA), Roma, Italy, [3]Istituto Nazionale di Geofisica e Vulcanologia (INGV), Roma, Italy, [4]Dipartimento di Ingegneria Civile e Meccanica (DICeM), Università degli Studi di Cassino e del Lazio meridionale, Cassino, Italy

Surface faulting and liquefaction are two earthquake-related effects to be considered in geological hazard assessment studies, particularly in application cases involving the construction or reconstruction of strategic buildings. The first effect is connected to the coseismic rupture on surface occurring along the active and capable fault, whereas the second relates to the ground seismic shaking and occurs mostly on sandy-silty grain sized deposits with shallow water table. Here, the results of investigations carried out in the Pagliare di Sassa village, nearby L'Aquila (central Italy), are presented, with the aim of shedding light on a potentially active and capable fault previously hypothesized at a site selected for the building of a school. The acquisition of paleoseismological, geophysical and geognostic data allowed to rule out the presence of the active and capable fault in the school area and to characterize several soft sediment deformation structures, interpreted as seismites related to two earthquake-induced paleoliquefaction events. Their occurrence has been linked through ceramic and radiocarbon dating. The seismites were used to determine the likely historical earthquakes (date, seismogenic source and magnitude), which in turn helped determine their occurrence contributing to the comprehension of the seismotectonic setting of central Italy. Lastly, the assessment of these local seismic instabilities, evidenced by the case study of Pagliare di Sassa, represents a key prerequisite for best practices in land and urban planning, devoted to the building of strategic edifice, such as a school. In such cases, the application of

palaeoseismological technique proves to be invaluable for mitigating the seismic risk.

KEYWORDS

surface faulting potential, paleoliquefaction, active tectonics, seismic microzonation, intermontane basin, Quaternary, central Italy

1 Introduction

Geological hazards associated with earthquakes, besides ground shaking, are coseismic instabilities, such as surface faulting, liquefaction, landsliding, sediment densification and differential compaction, and sinkholes (McCalpin, 2009). Within land and urban planning, these coseismic instabilities are addressed in seismic microzonation studies (e.g., Ohsaki, 1972; Fäh et al., 1997; SM Working Group, 2008; Molnar et al., 2020; Mori et al., 2020; Moscatelli et al., 2020; Yamazaki and Maruyama, 2020 Giallini et al., 2024). In the presented case study, located in the highly seismic territory of L'Aquila municipality (central Italy), surface faulting and liquefaction were specifically considered within a seismic microzonation project.

The surface faulting hazard, in the context of land and urban planning, necessitates the concept of "fault capability" (Galadini et al., 2012). This is defined as the coseismic motion along the main fault plane and potential minor associated faults, capable of inducing ground rupture and consequently displacing buildings, infrastructure, and pipelines. Within this framework, two key research areas are pivotal: (i) studying and modeling how faults impact infrastructure (e.g., Gazetas et al., 2008; Paolucci et al., 2010) and (ii) assessing surface faulting hazards, considering both regional (e.g., Guerrieri et al., 2009) and local scales, including the areal width of active fault setbacks (e.g., Boncio et al., 2012).

As regards Italy, after the 2009 Mw 6.3 L'Aquila earthquake, specific guidelines for active and capable faulting were subsequently issued (Technical Commission on Seismic Microzonation, 2015). These guidelines prescribe the zonation of portions of territories affected by the trace of faults that are considered active and capable, that is, potentially able to produce surface offset. Specifically, these guidelines define an active and capable fault as one that shows evidence of having affected terrains younger than the past 40 kyr. This time interval approximates the lower time boundary of the applicability of radiocarbon age determinations. Conversely, these guidelines define a potentially active and capable fault as one that shows geological evidence of activation during the Middle-Late Pleistocene but whose activity during the past 40 kyr is presently unknown.

These specific guidelines on active and capable faults have been produced because the causative fault of the 2009 Mw 6.3 L'Aquila earthquake, the so-called Paganica normal fault, produced surface faulting detectable for about 10 km, with the displacement of buildings, a regional motorway viaduct, and an aqueduct (e.g., Falcucci et al., 2009; Boncio et al., 2010; Galli et al., 2010). This evidence underscored the consideration of surface faulting as a major geological criticality to be addressed when managing land use in the main seismically active regions of the Italian territory.

Liquefaction, the second coseismic instability considered in the presented case study, is a phenomenon that occurs in water-saturated on mostly sandy-loose-cohesionless soils, which, when subjected to seismic stresses, temporarily lose their strength and behave like a fluid (Obermeier, 1996; Idriss and Boulanger, 2008; Boulanger and Idriss, 2014). Liquefaction in well-graded sandy gravels has also been observed at numerous global sites over the past decade (Salocchi et al., 2020; Rollins et al., 2021; Salvatore et al., 2022 and references therein). For evaluating the liquefaction susceptibility, several national building codes adopted the grain-size boundaries of the most liquefiable and potentially liquefiable soils proposed by Tsuchida and Hayashi (1971).

2 Geological and seismotectonic setting

After the 2009 Mw 6.3 L'Aquila earthquake, many seismic microzonation projects have been carried out, starting right from the epicentral area, involving the city of L'Aquila and the surrounding villages. This sector of the central Apennines is known since decades to be a highly seismically active region, affected by a large number of local historical seismic events with magnitudes of up to magnitude 6.5–7.0 (Rovida et al., 2022), generated by the activation of major active normal fault systems that affect this sector of the central Apennines (e.g., Boncio et al., 2010; Falcucci et al., 2009; Galli et al., 2010; Galli et al., 2011; Galli et al., 2022; Lavecchia et al., 2012; Moro et al., 2002; Moro et al., 2013; Moro et al., 2016).

The seismic microzonation projects consider the current knowledge on active tectonics and many active and/or potentially active and capable fault traces have been mapped at a appropriate scale. One of the primary objectives of these projects is to define the actual activity and capability of the preliminarily mapped potentially active faults, for which the knowledge was not exhaustive. Furthermore, other coseismic instabilities were considered, including, primarily, liquefaction.

The Pagliare di Sassa case study area (henceforth PSCSA) was also encompassed by the aforementioned seismic microzonation projects carried out after 2009 L'Aquila earthquake. PSCSA is located west of L'Aquila, where a potentially active and capable fault, known as the Pagliare di Sassa fault (henceforth PSF), was identified in the seismic microzonation map of L'Aquila Municipality pilot areas (Tallini et al., 2014). Along the PSF trace a site for a new school building was formerly selected (Nocentini et al., 2017) (Figures 1, 2).

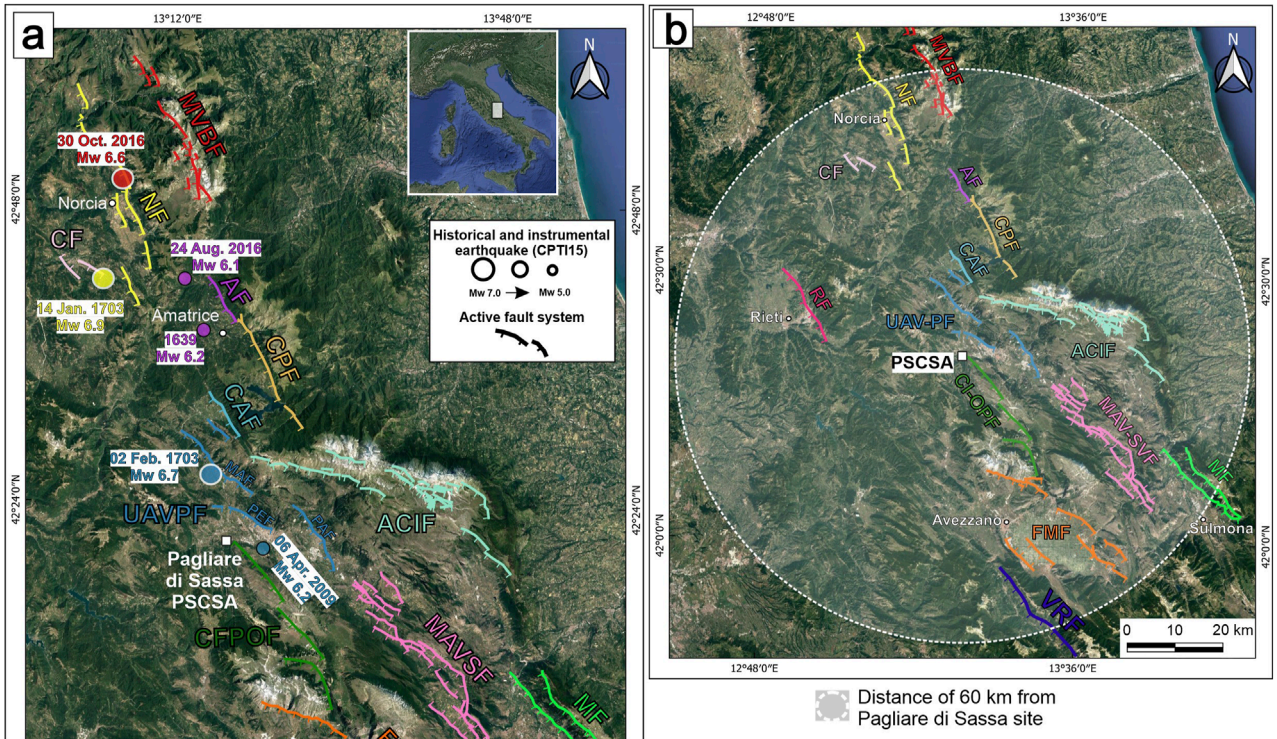

FIGURE 1
(a) Seismotectonic setting of central Apennines showing active faults system and the epicentres of large (6.0 < M < 6.7) historical and recent earthquakes with year of occurrence and magnitude: the different colours refer to the accountable active fault system. Active fault systems from literature (e.g., Falcucci et al., 2015; Galadini et al., 2018): MVBF: Mt. Vettore-Mt. Bove fault system; NF: Norcia fault system; CF: Cascia fault system; AF: Amatrice fault (Falcucci et al., 2016); CPF: Campotosto fault; CAF: Capitignano fault; RF: Rieti fault (Michetti et al., 1995); UAVPF: Upper Aterno Valley-Paganica fault system which comprises the Mt. Marine fault (MAF), Mt. Pettino fault (PEF) and Paganica fault (PAF); ACIF: Assergi-Campo Imperatore fault system (Galli et al., 2002; Galli et al., 2022; Galadini et al., 2003); CFPOF: Campo Felice-Pezza-Ovindoli fault system (Salvi et al., 2003); MAVSF: Middle Aterno Valley-Subequana fault system (Falcucci et al., 2011; 2015); MF: Mt. Morrone fault system (Gori et al., 2014); FMF: Fucino-Mt. Magnolia fault system (Galadini and Messina, 1994; Galli et al., 2012; Galadini et al., 2022); VRF: Roveto Valley fault (Maceroni et al., 2022). **(b)** Active faults for which paleoseismological evidence defines activation in historical times, consistent with the age of earthquake-induced paleoliquefaction events identified in PSCSA (Pagliare di Sassa case study area); AF, CPF, CAF, CFPOF, VRF represent active faults not considered from paleoseismological viewpoint in this work.

In the PSCSA, besides the presence of the potentially active PSF, an area indicated as prone to liquefaction is identified according to a preliminary version of L'Aquila seismic microzonation map (Tallini et al., 2014) (Figure 2). This aligns with evidence of several earthquake-induced paleo-liquefaction events observed in nearby areas to PSCSA (Martelli et al., 2012; Chiaradonna et al., 2021).

Given these conditions, this study aimed to investigate the PSCSA to unravel the activity of the PSF in the late Quaternary, specifically within the past 40kyr, as prescribed by the Italian Guidelines of active and capable faults (Technical Commission on Seismic Microzonation, 2015). The PSF appears to affect Early Pleistocene deposits but is seemingly sealed by Late Pleistocene alluvial fan sediments (Nocentini et al., 2017). However, uncertainties in this chronological assignment and the inherent rigidity of the 40 kyr timeframe (defined solely by a technical criterion in the Guidelines) preclude the dismissal of the PSF as inactive without conducting thorough geological investigations.

To this aim, several multi-methodological investigations were carried out in PSCSA. Their goals were not only to focus on the definition of the recent PSF activity but also to investigate the liquefaction potential. In view of a correct best practice on seismic risk management, these coseismic instabilities must be accurately considered due to the future construction of a new school building in PSCSA.

After introductory paragraphs dedicated to the geologic and seismotectonic framework of PSCSA, several methods and techniques applied are described, and the collected data are then presented. Specifically, we will show the

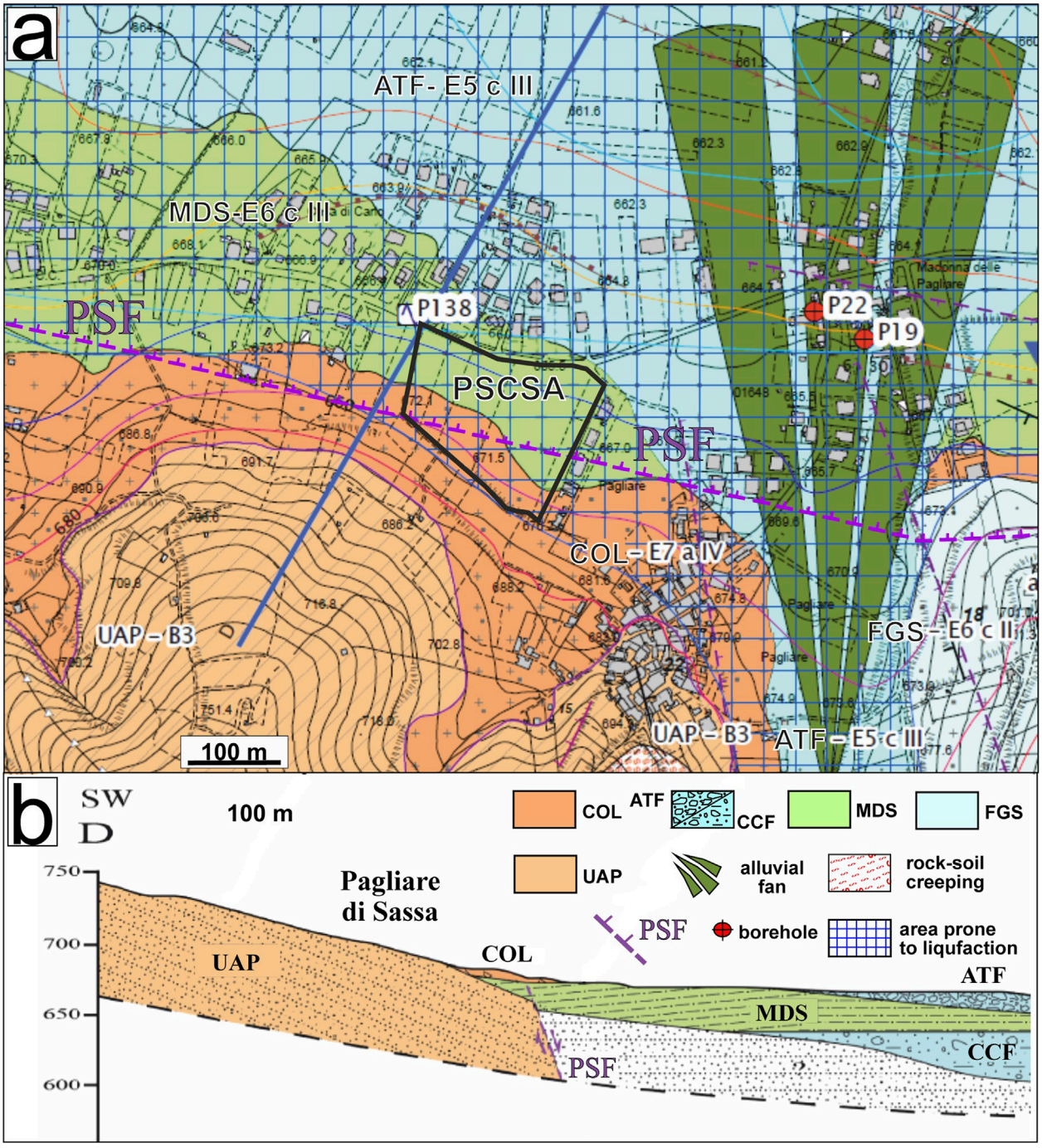

FIGURE 2
(a) Seismic microzonation map focusing on PSCSA [modified from Tallini et al. (2014)]; **(b)** geological section which shows PSF hypothesized to displace the boundary of MDS unit with the Miocene bedrock (UAP). PSF is mapped as sealed by recent colluvial deposits. ATF: alluvial deposit (Holocene); COL: colluvial deposit (Upper Pleistocene? - Holocene); FGS: Fosso Genzano System sensu (Nocentini et al., 2017), terraced alluvial deposit (Middle Pleistocene); MDS: Madonna della Strada System sensu Nocentini et al. (2017), alluvial deposit (Early Pleistocene); CCF: Colle Cantaro-Cave Formation sensu (Nocentini et al., 2017), alluvial deposit (upper Piacenzian-Gelasian); UAP: Upper Miocene substratum (sandstone and pelite). In the map (a) the unit names are classified following partly (Basi et al., 2012) and by using the following codes: lithotechnical unit (B3: layered rocks made up of alternating of rocky and pelitic levels; E5: gravelly sand; E6: silty-clayey sand; E7: sandy silt); matrix characteristics (a: rocky fragments; c: cohesive fine-grained fraction); thickening degree (II: moderately thickened, III: poor thickened, IV: loose).

results of ERT investigations, paleoseismological trenching, borehole coring, introductory and archeological and radiocarbon dating.

In the discussion and conclusions, the data collected through this multi-methodological approach, adopted in urban setting of seismically active region, will be examined and summarized,

respectively, from the perspective of defining whether the PSF must be considered as actually active and capable and of defining the possible active faults accountable for the paleoliquefaction events.

2.1 Geological and seismotectonic framework

Central Italy's current tectonic setting is the result of two main tectonic phases: (ii) the contractional phase (middle Oligocene to lower Pliocene) during which the formation of the Apennine fold and thrust belt occurred. This belt is a classic example of an ensialic post-collisional chain, characterized by an eastward-migrating piggyback sequence of the principal cover thrust-sheets (Cosentino et al., 2010; Cosentino et al., 2017). (ii) The extensional phase (Messinian-Quaternary). This phase, characterized by the opening of the Tyrrhenian Sea basin, led to the development of intermontane basins within the central Apennine chain (Carminati et al., 2010; Cavinato and De Celles, 1999).

In central Italy, the dominant extensional tectonic setting, relevant to the second phase, is characterized by SW- and S-dipping normal faults. These faults exhibit dip- and oblique-slip kinematics, resulting in complex graben or half-graben features corresponding to the intermontane basins, including the L'Aquila basin (Barchi et al., 2000). PSCSA is located within L'Aquila basin.

These basins were filled with lacustrine, slope, and alluvial deposits, beginning in the Upper Pliocene and continuing throughout the Quaternary to the present day (Cosentino et al., 2017). Many of the extensional faults, responsible for the formation of these basins, remain active and seismogenic. They are accountable for both present-day and historical seismic activity, as evidenced by seismological, GPS, and paleoseismological data (e.g., Boncio et al., 2004; Devoti et al., 2010; Pondrelli et al., 2006). These faults have the potential to generate earthquakes with maximum expected magnitudes of up to 6.5–7 (e.g., Galadini and Galli, 2000) (Figure 1).

The active normal faults of central Italy are split into a western set and an eastern one (Barchi et al., 2000; Falcucci et al., 2011). Several main historical earthquakes have likely been caused by the active extensional faults within the western set (Figure 1), such as the 1,349 (Mw 6.6), 1703 (Jan. 14; Mw 6.7), 1703 (Feb. 2; Mw 6.7) and 1915 (Mw 7.0) earthquakes (Rovida et al., 2022). This is supported by evidence, from the comparisons between the active faults pattern, the macroseismic damage distribution associated with these earthquakes and paleoseismological data (Galli et al., 2008 and references therein).

Conversely, the active faults of the eastern set, such as those of Mt. Vettore-Mt. Bove fault system (MVBF), Campotosto fault (CPF), Assergi-Campo Imperatore (ACIF), Upper Aterno Valley-Paganica fault system (UAVPF), Middle Aterno Valley-Subequana fault system (MAVSF) and Mt. Morrone fault (MF), defined each as a possible seismic gap since they did not activate during historical times (Galadini and Galli, 2000) (Figure 1). The 2016–2017 earthquake sequence (events with Mw up to 6.5), caused by two of the mentioned faults (MVBF and CPF; Figure 1), confirmed the preceding geological inferences.

Concerning the local seismotectonic setting of PSCSA and surroundings (Figure 1), the Mt. Pettino fault (PEF) represents the main active fault within ASB, bordering the NE slope of the basin. PEF dips to the south and southwest, extends for 14 km, and exhibits variable orientation. It pertains to the Upper Aterno Valley active fault system (UAVPF), whose movement throughout the Quaternary conditioned the tectonic and sedimentary evolution of the western portion of the L'Aquila basin (Figures 1–3). The UAVPF completely ruptured during the 2 February 1703 Mw 6.7 earthquake (Rovida et al., 2022; Figure 1), resulting in significant surface faulting, as observed through paleoseismological investigations (Galadini and Galli, 2000; Moro et al., 2002; 2013; Galli et al., 2011). PEF is in right en-échelon relationship with the near northernmost NW-SE trending 15 km-long extensional Mt. Marine fault (MAF). This latter is characterized by dip- and left oblique-slip (Moro et al., 2016). Significant surface faulting induced by the 2 February 1703 (Mw 6.7) earthquake has been recognized along the MAF, which caused considerable damage to L'Aquila town (Blumetti, 1995; Moro et al., 2002; Chiaradonna et al., 2021). To the east and southeast of L'Aquila basin, the seismogenic faults are the Paganica fault (PAF) and the Middle Aterno Valley-Subequana Valley fault system (MAVSF), which exhibit a NW-SE average direction and dip-slip kinematics (Galli et al., 2010; Figure 1). Geological, seismological and geodetic data show that the 6 April 2009 (Mw 6.3) L'Aquila earthquake (e.g., Hermann et al., 2011; Chiaraluce, 2012; Valoroso et al., 2013) was caused by the activation of the PAF, with an overall surface coseismic length of approximately 10 km (e.g., Falcucci et al., 2009; Galli et al., 2010; EMERGEO Working Group, 2010; Boncio et al., 2010; Gori et al., 2012; Moro et al., 2013).

2.2 Pagliare di sassa site (PSCSA) and fault (PSF)

PSCSA is placed within L'Aquila-Scoppito basin (ASB) sensu Nocentini et al. (2017), an E-W oriented asymmetrical graben. ASB, which is placed in turn within the broad L'Aquila basin, is filled up by chiefly Quaternary detrital deposits pertaining to alluvial and slope environments. It is bordered to the north mainly by the Mt. Pettino active fault (PEF in Figure 1; Galli et al., 2011) and, to the south, by its antithetic PSF, which is crossed by the Aterno River and its tributaries (Cosentino et al., 2017; Nocentini et al., 2017; Spadi et al., 2022) (Figures 1, 2).

Starting from the upper Piacenzian, ASB was filled up by a thick sequence of continental deposits laying via an unconformity surface onto the Upper Miocene terrigenous units and Meso-Cenozoic carbonate units (Figure 2).

ASB oldest post-orogenic deposits belong to the Colle Cantaro-Cave Formation (CCF in Figure 2) (upper Piacenzian-Gelasian) and include slope breccias, debris-flow deposits and matrix-supported alluvial conglomerates (Nocentini et al., 2017).

The Madonna della Strada Synthem (MDS), which is separated from the lower CCF by an unconformity boundary, is made up of clayey-sandy silts and sands. In the lower and middle part of MDS there are gravel levels with variable granulometry, from coarse to medium, and with a good rounding degree. Furthermore, levels of lignite and peaty pelite were found inside MDS (Mancini et al., 2012). The environment of MDS deposit can be referred to an alluvial system meandering within a wide and swampy floodplain.

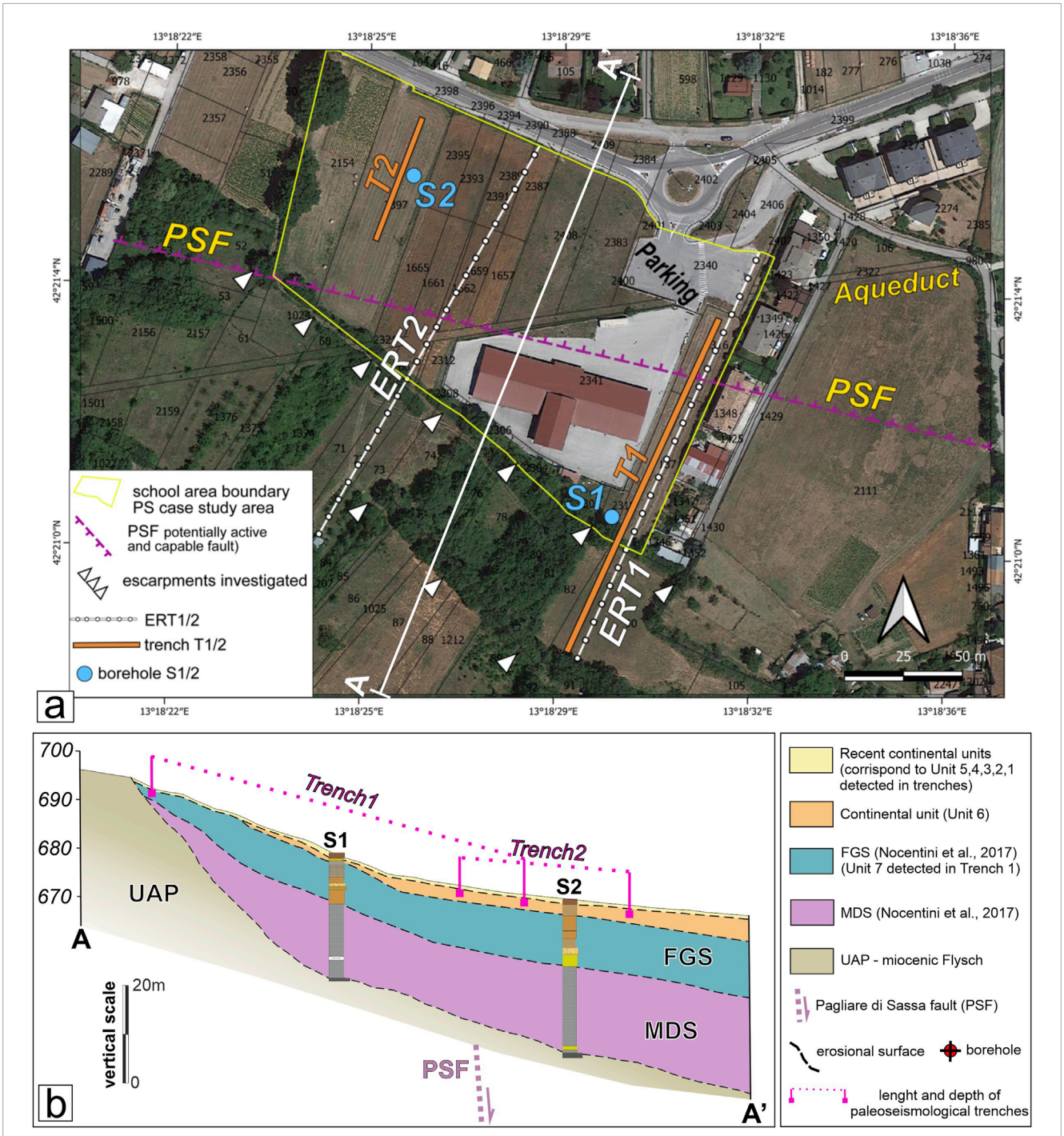

FIGURE 3
(a) Location of the investigations in PSCSA. ERT1 and ERT2: electrical tomography surveys; T1 and T2: paleoseismological trenches; S1 and S2: continuous core boreholes. PSF: presumed trace of Pagliare di Sassa fault. The A-A′ trace represents the topographic profile shown in the geological cross-section **(b)**; **(b)** geological section of PSCSA, realized by integrating data from trenches and boreholes.

MDS is dated back to the Calabrian age due to the reverse magnetic polarity of its deposits and the finding of specific mammalian fauna (Cosentino et al., 2017).

Above MDS, separated by unconformity boundaries, several deposits consisting of gravelly-sandy from Middle to Upper Pleistocene sediments of plain and alluvial fan environment (e.g., FGS) and late Middle Pleistocene calcareous breccia complete the filling of ASB (Antonielli et al., 2020; Nocentini et al., 2017; Tallini et al., 2019).

The most recent ASB deposits (Upper Pleistocene? – Holocene), outcropping in the study area, are represented by slope and colluvial (COL) deposits bordering the base of the surrounding reliefs and by the recent alluvial deposits of the Aterno River and its tributaries (ATF) (COL and ATF in Figure 2 are named together as ALCO).

PSF is a N-dipping extensional fault and borders the southern boundary of ASB graben, representing an antithetical fault of PEF (Moro et al., 2016; Galli et al., 2011). Along the PSF, evidence of Quaternary activity was detected. This activity lasted at least until the Middle Pleistocene and possibly into the Late Pleistocene (Nocentini et al., 2017).

PSF was considered in the seismic microzonation studies as a "Potentially Active and Capable fault" with an uncertain/presumed trace (Tallini et al., 2014) (Figure 2). As noted above, according to the Italian guidelines of seismic microzonation (Commissione tecnica per la microzonazione sismica 2015), an "Active and Capable" fault exhibits evidence of faulting within the last 40 ka, whereas a "Potentially Active and Capable fault" shows evidence of activity in the Middle-Late Pleistocene, but its activity over the last 40 kyr remains unknown and needs to be demonstrated.

In the section of the seismic microzonation map (Figure 2), PSF affects the MDS unit, but it is sealed by recent colluvial deposits (Late Pleistocene? - Holocene). In this context, Durante et al. (2017) demonstrate that FGS is displaced by PSF by approximately100 m east of PSCSA. Furthermore, an anthropic excavation reveals shear planes, associated with the PSF deformation zone, that affect the MDS. These shear planes are overlain by gravels of the CPF unit, dated to approximately 40 kyr (Cosentino et al., 2017) (Supplementary Figure 1). Therefore, the paleoseismological study performed at PSCSA was carried out considering: (i) that the 40 kyr constitutes the lower chronological boundary for the Italian definition of active and capable fault; (ii) that the aforementioned recent faulting is very close to this time boundary (Supplementary Figure 1); and (iii) the presence of two escarpments at the base of the slope, bordering the alluvial plain, which may represent fault-derived scarps (Figure 3).

Finally, it should be noted that the fault is not mapped in the geological sheet no 358 Pescorocchiano of CARG Project (ISPRA, 2010) (scale 1:50.000), in the ITHACA Catalog (ITHACA Working Group, 2019) and in the DISS Database (DISS Working Group, 2018).

3 Materials and methods

To assess the presence and the recent activity of PSF in PSCSA, several investigations were conducted, including two electric resistivity tomography profiles (ERT), two boreholes (named S1 and S2) and two paleoseismological trenches (hereafter Trench 1 - T1 and Trench 2 – T2) (Figure 3).

Firstly, geophysical and paleoseismological surveys were carried out along the eastern and western edges of PSCSA, orthogonal to the presumed PSF fault trace, to obtain a complete picture of the investigated area. It should be noted that the location of the investigations was also constrained by logistics and the presence of underground utilities and an important buried aqueduct. The general characteristics of the ERT are as follows: i) acquisition method: Wenner; ii) electrode numbers: 64; iii) length: 189 m; iv) unit electrode spacing: 3 m. Trenches T1 and T2 are 150 m and 50 m long, respectively, and reach a depth of approximately 2–2.5 m below the ground surface, with an approximate width of 3 m. Moreover, to achieve more robust chrono- and litho-stratigraphic information of the continental units detected in the paleoseismological trenches and to improve the geological setting of PSCSA, continuous coring 30-m deep boreholes S1 and S2 were drilled at the hanging wall and the footwall of PSF, respectively. The Miocene substrate was encountered at the bottom of the S1 and S2 boreholes.

Chronological information about the deposition of continental units intersected by the borehole and exposed in the trenches was acquired by dating archaeological pottery fragments (found in the trenches) and by radiocarbon dating by Beta Analytic laboratory (https://www.radiocarbon.com) on samples collected from the trenches and boreholes cores.

The laser scanner of the two trenches and the photogrammetric survey of the most interesting portions of Trench 2 were conducted. The instrument used was the FARO Focus S 70 phase difference laser scanner, featuring a complete field of view (FOV) of 360° × 300° and an integrated HDR camera. To obtain a homogeneous point cloud, the scan stations were chosen to maintain a constant distance from each other. Specifically, 32 and 14 scans were acquired for Trenches 1 and 2, respectively. The laser scans were positioned between Trench 1 and 2 at an average distance of 5 and 4 m, respectively. The adopted resolution (number of points acquired per rotation) was 1/4 and 1/5 - corresponding to a point spacing of 6.1 and 7.7 millimiters at 10 m from the instrument, respectively.

4 Results

4.1 ERT investigations

Prior to digging the paleoseismological trenches, two electrical resistivity tomographies (hereafter ERT 1 and ERT2) were performed.

The ERTs in general highlight medium-to-low resistivity values, ranging from 5 to 200 Ωm, which are indicative of the clayey-sandy and arenaceous lithologies encountered in the two trenches and in the boreholes S1 and S2, as described below.

In ERT1, two resistivity layers were identified: the superficial layer ("a" in Figure 4) exhibits a resistivity of 55–75 Ωm, while the underlying layer ("b" in Figure 4) has a resistivity of 15–40 Ωm. Furthermore, in the sector where S1 borehole was drilled at approximately 30 m depth, a change in resistivity from approximately 80–200 Ωm is observed ("c" of Figure 4).

ERT2 detects two continuous layers: the shallow one ("d" in Figure 4), a few meters thick, has a resistivity around 60–80 Ωm, the underlying one ("e" in Figure 4), about 5 m thick, with a resistivity equal to 20–35 Ωm.

The general trend of the recorded resistivities does not show lateral contacts or abrupt changes extending from the surface to the depth. Furthermore, the lateral continuity of the shallow resistivity layers ("a", "b", "d" and "e" in Figure 4) is evident. These observations do not suggest the presence of discontinuities in the primary attitude of the layer, possibly related to displacements caused by faults.

4.2 Paleoseismological trenching and boreholes

To verify the presence and recent activity of PSF, trenches T1 and T2 were excavated across the scarp (Figure 3). The trenches

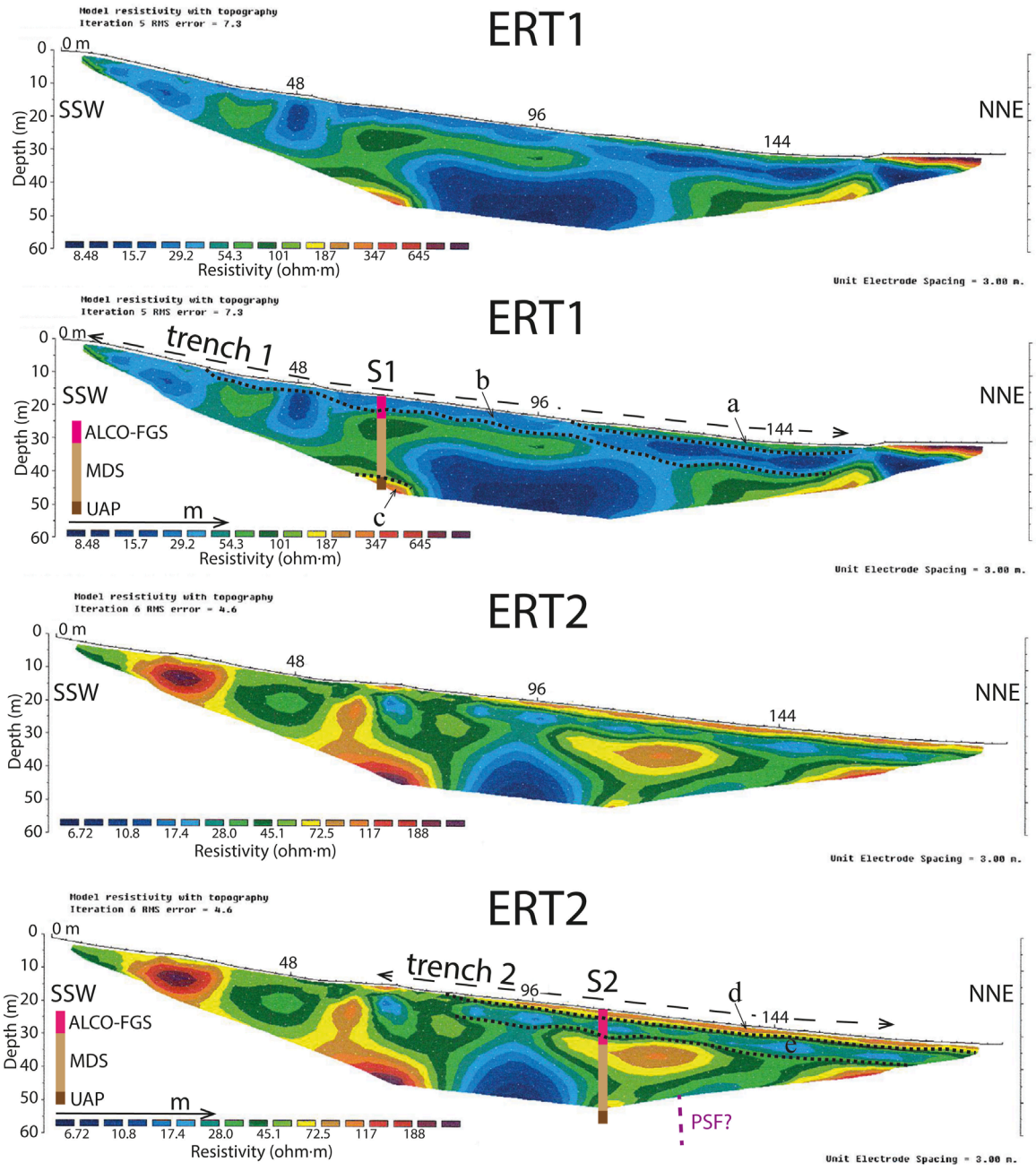

FIGURE 4
ERT1 and ERT2. For the location see Figure 3. S1 and S2 refer to the boreholes a, b c and d refer to resistivity layers recognized in the ERT. S1/S2 stratigraphic logs of boreholes S1 and S2 (see Figure 3): ALCO (COL and ATF are named together as ALCO): sand, silt and gravel, alluvial and colluvial deposit (Holocene-Upper Pleistocene); FGS: sand, silt and gravel, Fosso Genzano Synthem (Middle Pleistocene); MDS: silt and sand, Madonna della Strada Synthem (lower Pleistocene); UAP: arenaceous-pelitic rocks (Upper Miocene). PSF: Pagliare di Sassa fault.

overlapped by a few meters to address logistical constraints and ensure the investigation of the entire site.

The two paleoseismological trenches revealed a stratigraphic sequence of alluvial and colluvial units. The deposition of these units is related to the surface water dynamics in the local alluvial plain and to erosion and depositional processes on the slopes around the study area (Figures 5–7).

Chronological information about the deposition of units was acquired by (i) archaeological determination of pottery fragments (Supplementary Table 1; Supplementary Figure 2); (ii) radiocarbon dating of charcoals and organic-rich samples (Supplementary Table 2).

Based on the stratigraphic relationships and correlations between the continental units identified in both trenches, seven main sedimentary units have been distinguished. They are described here from the lowest (oldest unit exposed by Trench 1) to the uppermost unit (Figure 8).

Unit 7 (FGS unit, Middle Pleistocene): it consists of an alternation of decimetric sub-horizontal levels of silt (Munsell colour: 7.5 YR 6/1 – gray) and sands (colour Munsell: 7.5 YR 6/8

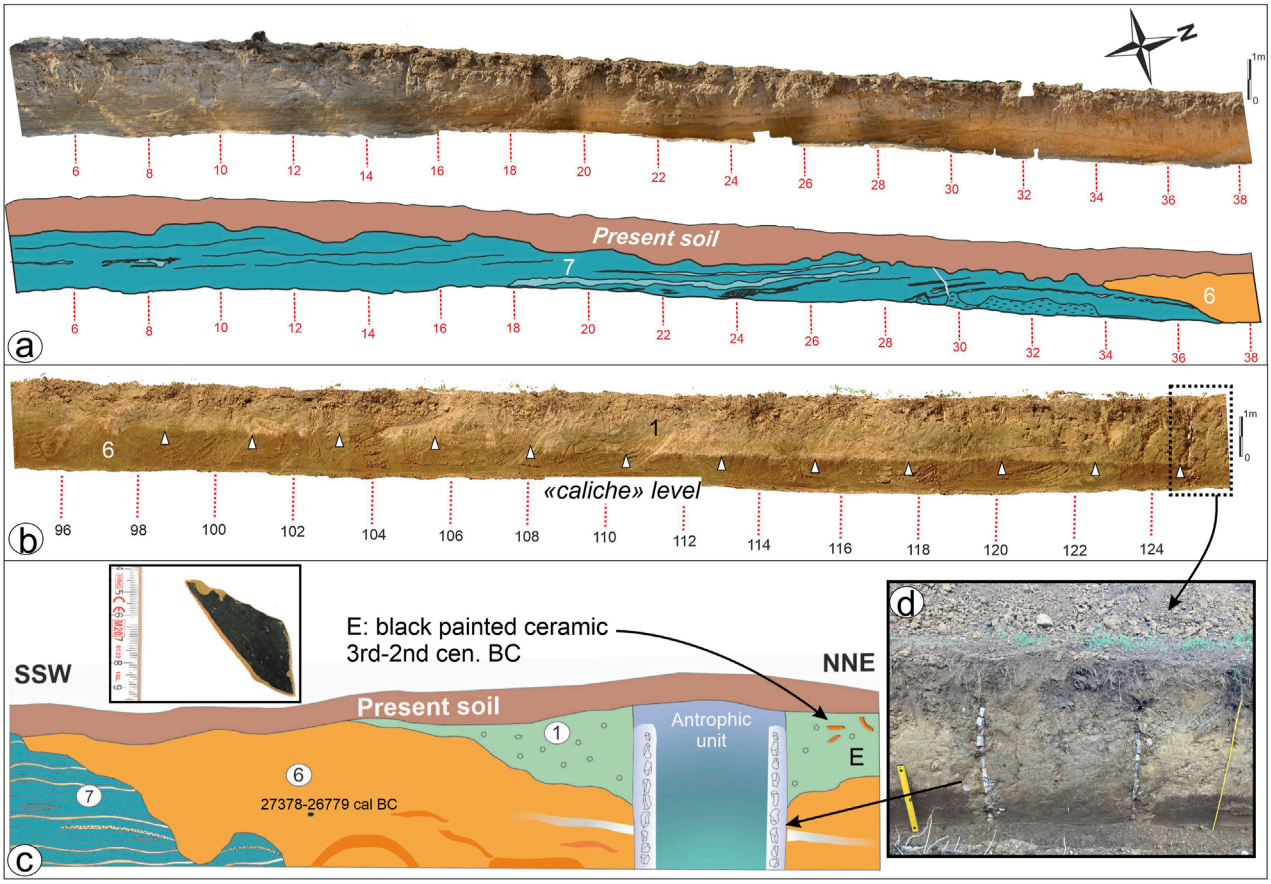

FIGURE 5
(a) Photomosaic (top) and stratigraphic interpretation (bottom) of the portion (6–38 m) of the Trench 1, western wall. The numbers refer to the units outcropping in trench. Unit 7: FGS unit (Middle Pleistocene). The units 1 and 6 refer to silty and sandy Holocene deposits of low-energy alluvial plains or fans. For the detailed description of the units see the text. The dating of charcoal sample and pottery shards (E) are reported in Supplementary Figure 1; Supplementary Table 1; **(b)** Photomosaic of the portion (96–124 m) of the Trench 1 western wall that shows the caliche level (white triangle) and the southern wall of anthropic well; **(c)** simplified stratigraphic model of Trench 1; sample SASSA_CARB_1 age (Supplementary Table 2): 27378–26779 cal BC. **(d)** The picture shows a detail of the historical water well (the structure was made of piled-up, rectangular-shaped rock blocks) detected at 124 m and 126 m which was filled by anthropic carryover.

– reddish yellow). Horizontal and inclined laminations, ripple and cut-and-fill structures indicate a fluvial braided plain and alluvial fan environment. In Trench 1, a level of sub-angular centimetric carbonate clasts marks a NE-dipping erosion surface that separates unit 7 from unit 6 (PG: 34–37 m) (Figure 5). The sedimentological and depositional characteristics, along with the local morpho-stratigraphic setting, allow this deposit to be correlated with the FGS unit (Middle Pleistocene) (Centamore and Dramis, 2010; Nocentini et al., 2017) (Figure 2).

Unit 6: silty-clayey and sandy massive deposit (Munsell colour: 2.5 Y 6/6 – olive yellow; 2.5 Y 7/8 – yellow) often characterized by mottles, patinas and nodules of Fe and Mn oxides. Small red slags of volcanic origin were found, and some organic sediments were collected and dated with 14C method at 27,378–26779 cal BC (Supplementary Table 2). The lithofacies and grain size of the sediment allow us to refer unit 6 to a deposition in a low-energy alluvial plain environment. In Trench 1, starting from about 95 m, unit 6 shows a carbonate caliche level, most probably related to vertical fluctuations of an ancient water level (Figure 5B). In Trench 1, the lateral continuity of unit 6 is interrupted between the PG 124 m and 126 m by a well dug by hand which was later buried and filled in by anthropic deposit in the 1950s as suggested also by local witnesses (Figures 5C, D).

Units 5, 4, 3 and 2 are found in Trench 2, especially between PG 20 and 38 m. These units consist of silty and sandy deposits of low-energy alluvial plains or fans, exhibiting significant soft sediment deformation-type structures (Figures 6, 7).

Unit 5: it comprises clayey silt (Munsell colour: 7.5 YR 4/6 – strong brown) with variable thickness, overlying unit 6 (Figures 6, 7). This unit contains numerous pottery shards and charcoal shreds, one of which was sampled and dated with 14C method at 1,507–1,407 cal BC (Supplementary Table 2). Given the sedimentological characteristics and the abundant organic material, this unit can be attributed to pedogenic processes affecting unit 6. Evident eroded mushroom-like structures are observed within it.

Unit 4: it outcrops between PG 32 m and 34 m (Trench 2) (Figures 6, 7). It is a body embedded within units 5 and 6 and overlain by unit 3. The deposit exhibits a sandy-silty

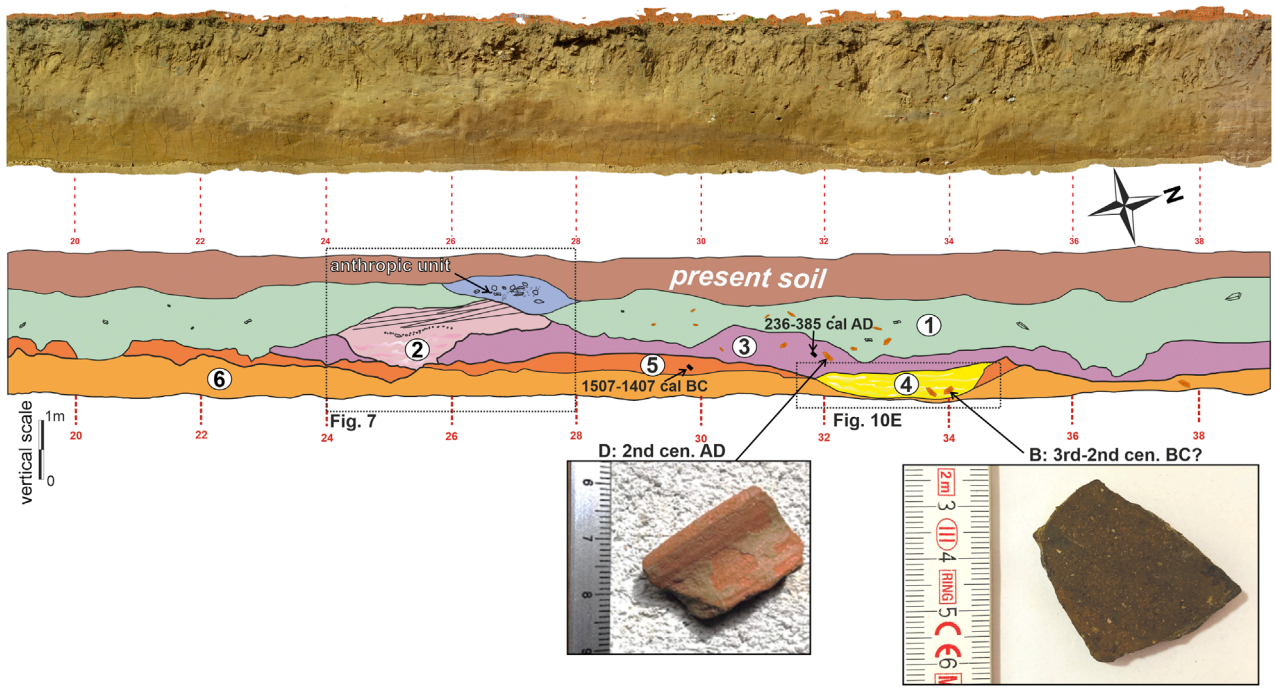

FIGURE 6
Photomosaic (top) and stratigraphic interpretation (bottom) of the stratigraphic portion (20–38 m) of the Trench 2, western wall. The numbers refer to the units outcropping in trench. The units from 1 to 6 refer to silty and sandy Holocene deposits of low-energy alluvial plains or fans that show significant soft sediment deformation-type structures. For the detailed description of the units see the text. The dating of significant charcoal samples and pottery shards (B and D) are reported in Supplementary Figure 1; Supplementary Table 1. Sample SASSA_CARB_4 age: 236–385 cal AD; sample SASSA_CARB_5 age: 1,507–1,407 cal BC (Supplementary Table 2). The dotted line rectangles refer to Figures 7, 10.

grain size (Munsell colour: 10 YR 6/6 – brownish yellow) with soft-sediment deformations and sandy dikes. Fragments of ceramic material were also found in its lowermost part (Supplementary Table 1; Supplementary Figure 2).

Unit 3: it consists of a silty-clayey massive deposit (Munsell colour: 7.5 YR 6/4 – light brown) (Figures 6, 7). Significant soft-sediment deformations, such as pseudonodules, load structures, and disturbed laminations were found. A fragment of an olla hem from the Roman period was discovered in unit 3, which can be ascribed to a chronological range between the 1st–2nd century AD (Supplementary Table 1; Supplementary Figure 2). A charcoal sample was collected very near the olla hem and dated with 14C method at 236–385 cal AD, strengthening the archaeological dating (Supplementary Table 2).

Unit 2: the deposit is an E-W trending channeled sandy-silty body underlying units 3 and 5 and covered by unit 1 (Figures 6, 7). It has been divided into two sub-units which show different sedimentary structures. Unit 2b is a sandy deposit (Munsell colour 2.5Y 7/4 – pale yellow) with laminations, cut-and-fill structures and significant soft-sediment deformations such as disturbed laminations, mixed and disturbed layers, mushroom structures, pseudonodules and two whitish sandy dikes. The overlying unit 2a is made up of light brown sands (Munsell colour 2.5Y 8/4 – pale yellow) with flat-parallel laminae and scattered centimeter-long calcareous clasts. It does not exhibit soft-sediment deformations. The two dikes of unit 2b seem to be sealed by the overlying unit 2a.

Unit 1: sandy colluvial deposit (Munsell colour 2.5Y 8/6 – yellow) containing angular and rounded carbonate clasts and abundant fragments of pottery and bricks (Figures 5–7; Supplementary Table 1; Supplementary Figure 2). Unit 1 was locally affected by anthropogenic excavations.

The two trenches did not reveal any shear planes or discontinuities that could be associated with tectonic dislocations after the deposition of the stratigraphic units. In fact, the units exhibited evident stratigraphic lateral continuity, consistent with primary sedimentary bedding, and they are only locally interrupted by structures related to anthropogenic activity and low-slope erosional surfaces.

Considering the age of the charcoal samples obtained by radiocarbon dating and the historical age of the pottery shards, it was possible to rule out surface faulting events at least in the last 25 kyr. However, since the time span (25 kyr) is more recent than the chronological interval (40 kyr) recommended by the Italian Guidelines for Microzonation studies (Commissione tecnica per la Microzonazione Sismica, 2015) to exclude the presence and recent activity of PSF, two continuous core boreholes were drilled near Trench 1 and Trench 2 (boreholes S1 and S2, respectively), each reaching depth of 30 m below ground level (Figures 5, 6). Boreholes S1 and S2 were drilled in the PSF footwall and hanging wall, respectively, to investigate possible tectonic dislocations of deposits older than 25 kyr (Figure 9). To improve the chronostratigraphic setting, a sample of plant remains, obtained at 19 m depth in borehole S1 yielded an age of >43,500 years using the

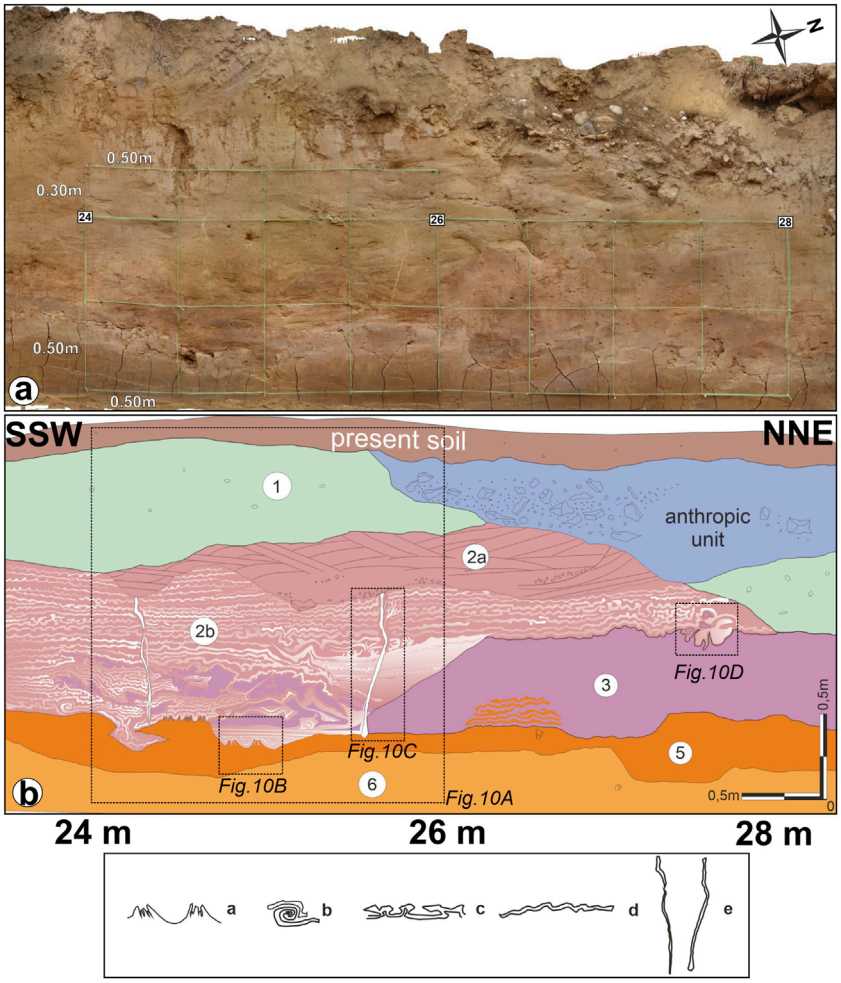

FIGURE 7
Photomosaic **(a)** and stratigraphic interpretation **(b)** of the stratigraphic portion (PG: 24–28 m) of the Trench 2, western wall. See Figure 6 for the location. The green line represents the metric grid created for stratigraphic interpretation. The numbers refer to the units outcropping in the trench. The units from 1 to 6 refer to silty and sandy Holocene deposits of low-energy alluvial plains or fans that show significant soft sediment deformation-type structures. For the detailed description of the units see the text. Soft sediment deformations (seismites) sensu Moretti and Sabato (2007) and Rodriguez-Pascua (2000): a-pillow structures (?); b-pseudo-nodules; c-mushroom shape structures; d-varved laminations; e–sandy dikes.

14C method (Supplementary Table 2). In two samples taken in the borehole S2 at 1.4–1.6 m and 11.70 m depth, the grain size analysis was conducted to determine the sedimentological characteristics of the shallow alluvial deposit (units 2a and 2b) (Figure 9).

The stratigraphy outlined from the S1 and S2 borehole logs, compared with the local geological setting (Centamore and Dramis, 2010; Nocentini et al., 2017), allowed the recognition of the Quaternary FGS and MDS Synthems. At the borehole bottom, greyish well-cemented sandstone was encountered, which outcrop in neighboring areas, particularly just upstream of PSCSA. It is attributable to UAP, the Upper Miocene synorogenic terrigenous unit (Centamore and Dramis, 2010) and corresponds to the pre-Quaternary substratum of PSCSA. Regarding the interpretation in terms of presence/absence of shear planes in the investigated area, the stratigraphic settings derived from the two boreholes will be discussed in the next section.

No very shallow water table was encountered during the drilling of S1 and S2 boreholes. This observation is of significant importance regarding the potential for liquefaction phenomena (see Section 5.2 ahead).

5 Discussion

5.1 Assessing surface PSF faulting in PSCSA

Geophysical investigations (ERT1 and ERT2) primarily evidenced several shallow continuous resistivity layers. Paleoseismological trenches (T1 and T2) enabled the identification of these layers as primarily related to alluvial/slope-environment deposits. In this regard, it is possible to exclude the tectonic origin of the two escarpments at the base of the slope, which could be interpreted as a morphological indicator of PSF activity. These escarpments are, therefore attributed to other phenomena of non-tectonic origin, considering the local geomorphological setting, such as fluvial erosion, slope dynamics and anthropogenic

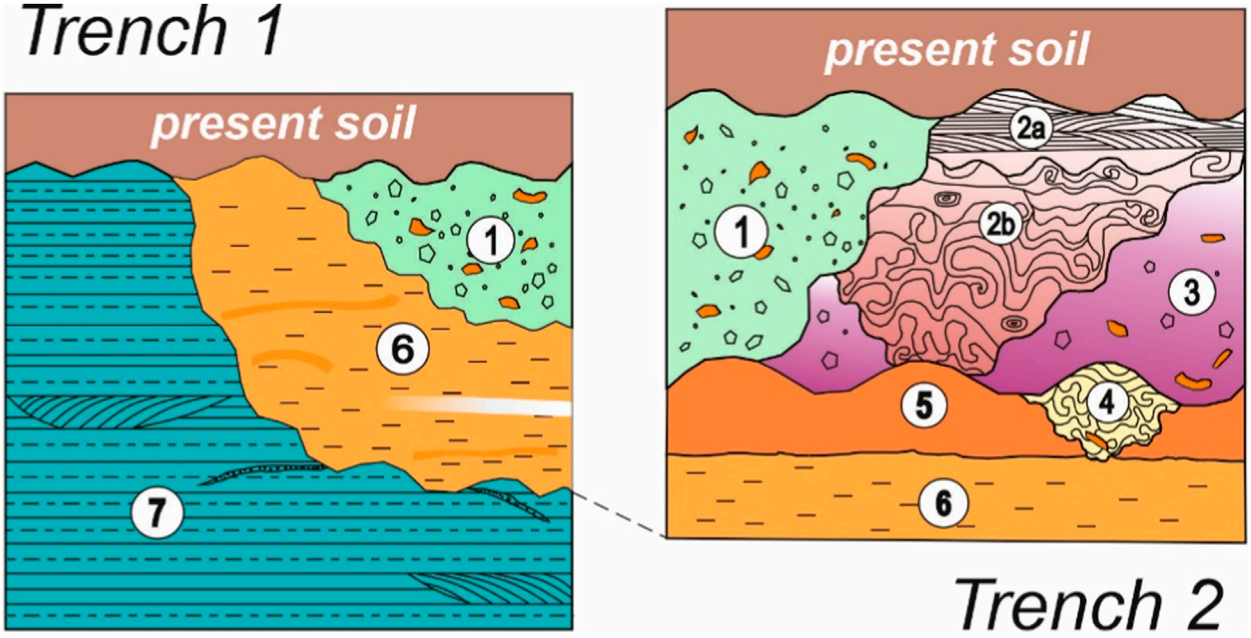

FIGURE 8
Stratigraphic scheme (not in scale) of the continental units exposed by the two trenches. The numbers refer to the units outcropping in trenches 1 and 2. Unit 7: FGS unit (Middle Pleistocene). The units from 1 to 6 refer to silty and sandy Holocene deposits of low-energy alluvial plains or fans that show significant soft sediment deformation-type structures. For the detailed description of the units see the text.

features. Consequently, these data suggest that the presence of escarpments cannot indicate the presence of faulting at or close to the ground surface.

From a chronological perspective, the analyses of the paleoseismological trenches have ruled out faulting events within the last 25 kyr. This is because unit 6, the oldest Late Pleistocene-Holocene unit found in the trenches, dated to 27378–26779 cal BC, remains continuous and is not disrupted by shear planes (Figure 5). Furthermore, considering the mean recurrence interval of major seismogenic fault in the central Apennine, typically ranging from 1,500 to 2000 years (Galadini and Galli, 2000; Galli et al., 2008), a 25 kyr timeframe should encompass a substantial number of possible faulting events (see Galadini et al., 2012 on this aspect). However, according to the aforementioned Italian guidelines for seismic microzonation, this time interval (25 kyr) is considered more recent than the required 40 kyr to definitively exclude surface faulting events. This is especially important given that the PSF displaces the MDS deposits (Early Pleistocene) not so far from PSCSA (Supplementary Figure 1). Therefore, to ensure safety, the implementation of boreholes was deemed necessary to assess vertical displacement related to the PSF activity within older stratigraphic units.

The shallow stratigraphy of the two boreholes is comparable to that recognized in the two trenches, up to a depth of 10–15 m. The boreholes encountered at greater depths the boundary between FGS and MDS, at 7 m in S1 and 11 m depth in S2 and the deeper boundary between MDS and UAP at 25 m in S1 and 32 m depth in S2.

The differences in depth of the boundary between FGS onto MDS and MDS onto the UAP in the two boreholes are about 12 m and 16 m, respectively. Considering the two boreholes are about 100 m apart, the dip towards the northeast of the FGS-MDS and MDS-UAP boundaries is almost the same, at approximately 7.5° and 9°, respectively. These very low values can be simply explained by the morpho-stratigraphic setting of the area, in which the erosional and depositional features of the continental units are consistent with the dip towards the alluvial plain, as would be expected at the basin boundary (Figure 3).

In this regard, the stratigraphic correlation of FGS-MDS and MDS-UAP boundaries, combined with the results obtained from the paleoseismological trenches, allowed us to rule out dislocations in the entire stratigraphic sequence starting from the Miocene bedrock (UAP). This indicates the absence of surface faulting since a period much longer than the last 40 kyr and, therefore, the recent activity of PSF in PSCSA. Thus, even though the important seismogenic faults of Mt. Marine, Mt. Pettino, and Paganica, located close to the study area, have been activated several times in the last 25 kyr, generating surface faulting (Galli et al., 2011; Moro et al., 2013), traces of this activity for the PSF, considered to be antithetical to the Mt. Pettino fault, have not been detected.

5.2 The soft-sediment deformation: hint for paleoliquefaction phenomena

Paleoseismological trenches revealed significant soft-sediment deformations affecting the units exposed in the trenches. More precisely, these structures were recognised in units 5, 4, 3, 2b of Trench 2 (PG: 22–34 m) (Figures 5–7). The identified post-depositional deformation structures are similar to those described

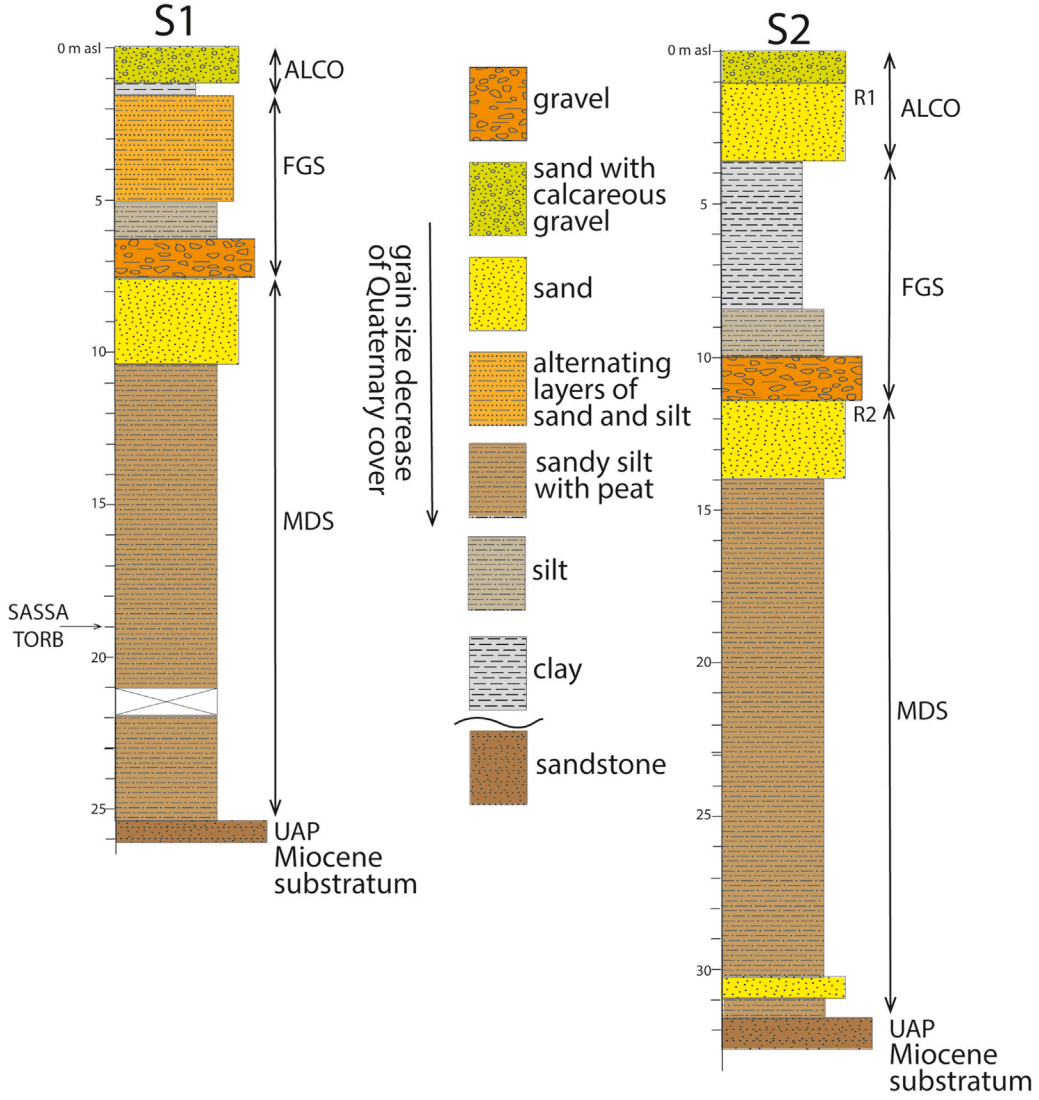

FIGURE 9
Stratigraphy logs of the two continuous core boreholes S1 and S2 (for the location see Figure 3). ALCO- shallow alluvial e colluvial deposit, ATF and COL Aterno River Synthem (Holocene), units 1–6 of Trench 1 and 2; FGS- Fosso Genzano Synthem (Middle Pleistocene), unit 7 of the Trench 1; MDS- Madonna della Strada Synthem (Early Pleistocene); UAP- sandstone (Upper Miocene). The stratigraphic units refer to Nocentini et al. (2017). R1 (1.4–1.6 m depth) R2 (11.70 m depth): samples on which the grain size analysis was carried out; SASSA_TORB: sample dated with 14C method (age: >43,500 BP) (Supplementary Table 2). S1 and S2 borehole elevations are 674 and 665 m asl, respectively.

in Moretti and Sabato (2007) and in Rodriguez-Pascua et al. (2000). They include loop bedding, boudinage-like structure, disturbed varved laminations, mixed layers without fluidization, mushroom-like silts protruding into laminites, large-scale load structures, mixed and disturbed layers with fluidization, pseudonodules, pillow structures, sand dikes and water escape structures (Figure 10). For the sandy dikes, the geometry has been reconstructed by analyzing both the trench walls and the eastern terrace of Trench 2 (Figure 11).

With the achieved 3D view, we estimated two main orientations of the sandy dikes: NNE-SSW and NW-SE. Moreover, both sandy dikes were likely formed simultaneously as they are filled with the same whitish, fine sandy sediment, and at their intersection, the deposit is homogeneous.

In literature, soft-sediment deformations such as those described are related to liquefaction phenomena in water-saturated silty-sandy deposits (Obermeier, 1996; Rodriguez Pascua et al., 2000; Moretti and Sabato, 2007). According to Moretti and Sabato (2007), the mechanisms that trigger liquefaction, and thus the formation of soft-sediment deformations, may be due to lithostatic loading or earthquakes.

To support the hypothesis that the observed soft-sediment deformations mentioned above were generated by earthquakes, the following arguments can be presented:

(1) Conditions potentially predisposing to liquefaction were found in PSCSA: (i) shallow sandy levels with high probability to liquefaction (Figure 12); (ii) the caliche level exposed in the

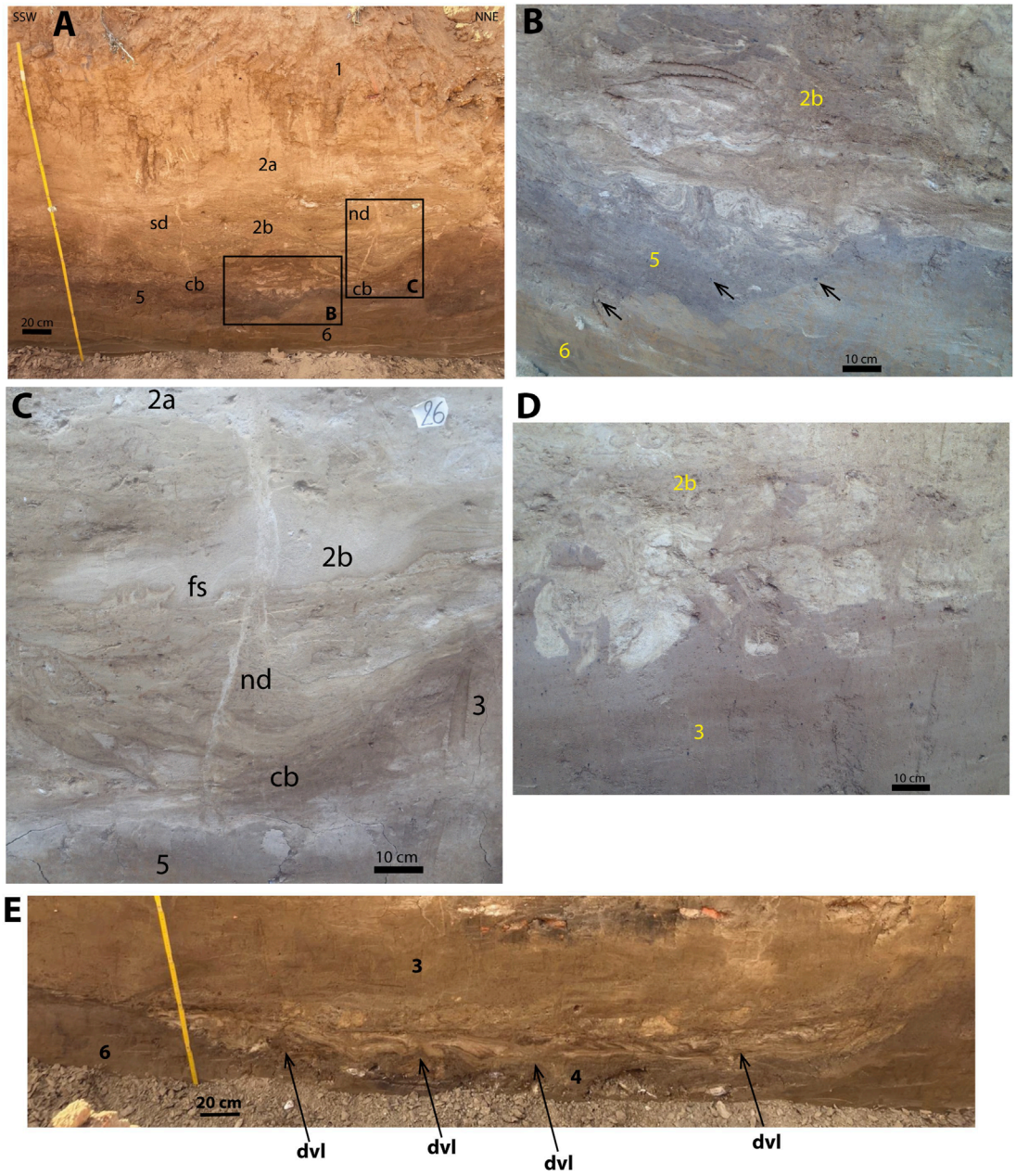

FIGURE 10
Pictures are located in Figure 7. **(A)** south (sd) and north (nd) sand dikes of unit 2b (Trench 2, PG: 24–26 m; units 1, 2a, 2b, 5 and 6). Note how both dykes (sd and nd) start from two E-W oriented channelized bodies (cb) and reach the same level upwards (unit 2a); the pictures **(B, C)** are located also in the picture **(A)**. **(B)** Eroded mushroom-like structures (Trench 2, PG: 25.20 m unit 2b, 5 and 6). The black dots in unit 5 refer to charcoal shreds (see arrows). **(C)** Sand dike (nd: north dike) and fluidization structure (fs) (Trench 2, PG: 25.70 m units 2a, 2b, 3 and 5); cb: channelized body. **(D)** Pseudonodules (Trench 2, PG: 27.40 m unit 2b and 3). **(E)** Deformed varved laminations (dvl) (Trench 2, PG: 32–34 m unit 4); dvl: deformed varved laminations.

Trench 1 testifies to very shallow fluctuations of the Holocene water table in sandy deposits (Figure 5). This setting highlights the liquefaction-prone conditions in the past (Figure 5).

(2) at a site located very close to PSCSA (500 m east), Chiaradonna et al. (2024) demonstrated that surface alluvial deposits, very similar to those of units 2a and 2b in PSCSA, can give rise to liquefaction. They assessed the liquefaction potential, using geotechnical methods based on different *in situ* test results (CPTU, DMT, Vs.).

(3) According to Obermeier (1996), to verify whether the soft-sediment deformations are caused by earthquakes, it is necessary not only that the lithological and hydrodynamic characteristics of the deposit are susceptible to liquefaction but also, and most importantly, that the structures are comparable to those documented in other geological settings located a few kilometres away from the investigated site, as a consequence of an occurring earthquake. In this regard, paleoliquefaction events are well documented in the

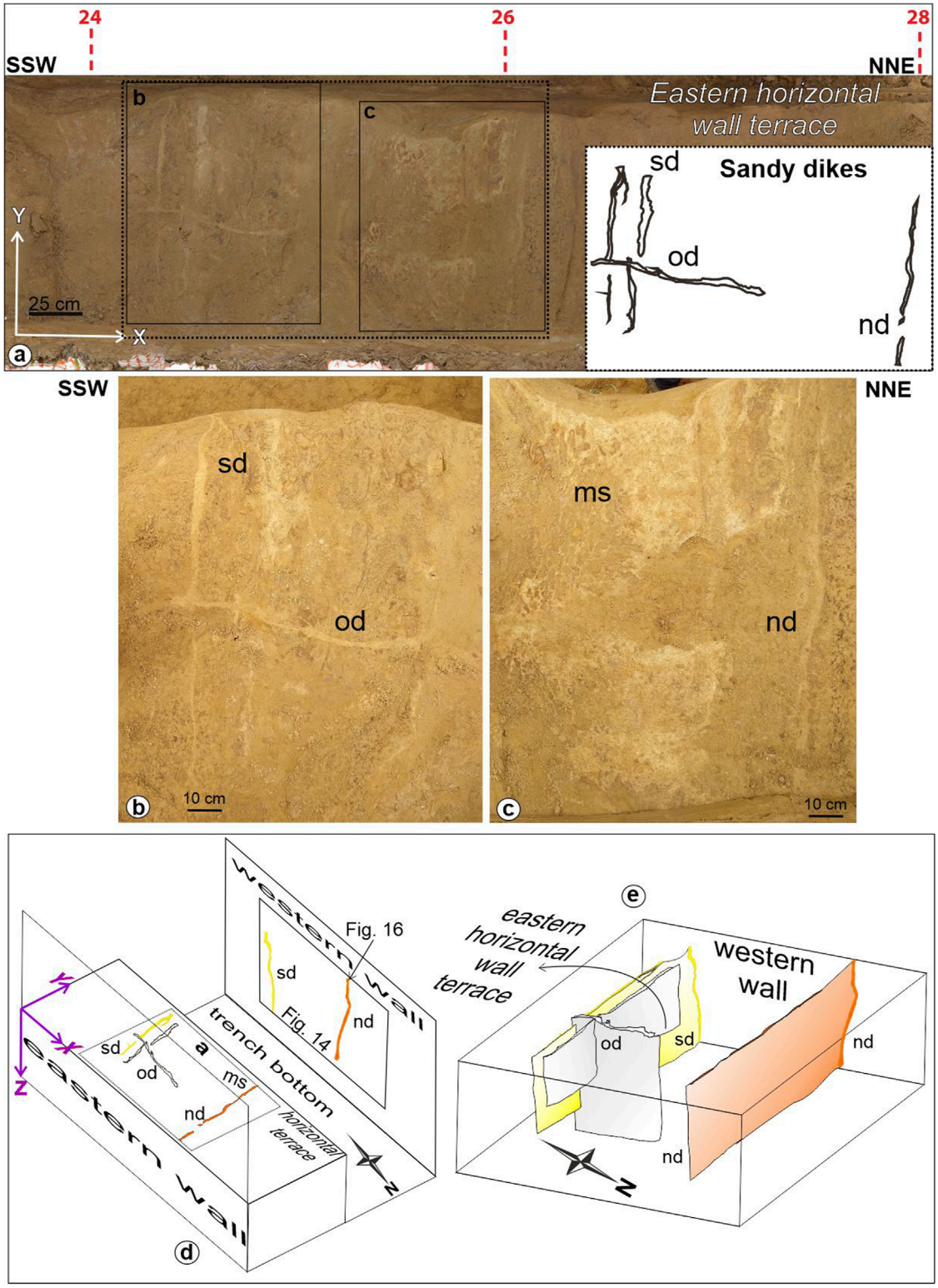

FIGURE 11
(a) Plan view of sandy dikes located along the eastern horizontal wall terrace of Trench 2 (PG: 24–26 m); **(b, c)** detail of the eastern horizontal wall terrace; scheme **(d)** and 3D view **(e)** of the sandy dikes; sd: south dike; nd: north dike; od: orthogonal dike; ms: eroded mushroom shape structures (?).

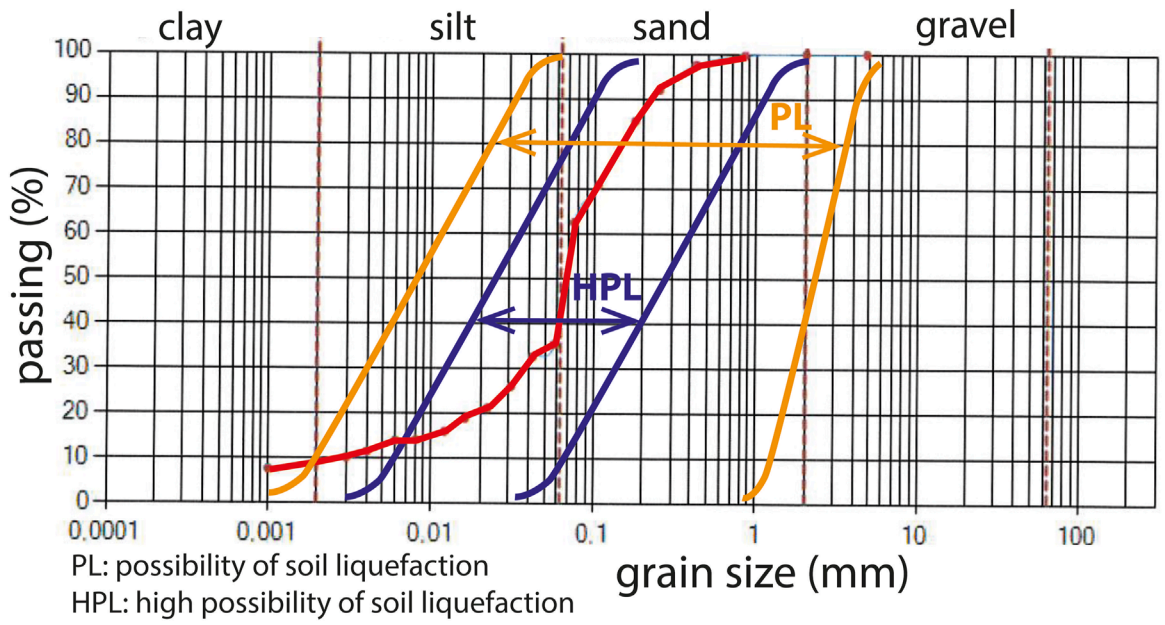

FIGURE 12
Grain size curve (red line) of sample taken in the historical or protohistoric alluvial deposit (units 2a and 2b) at 1.40–1.60 m below ground level in the borehole S2 (Figure 9). HPL: high possibility of soil liquefaction; PL: possibility of soil liquefaction (Sherif et al., 1977).

literature at several sites near PSCSA. More precisely, some of these paleoliquefaction events have been recognised within a radius of 50 km from PSCSA (Oddone, 1915; Blumetti, 1995; Galli, 2000; Monaco et al., 2011; Martelli et al., 2012; De Martini et al., 2012; Storti et al., 2013; Boncio et al., 2018; 2020; Iezzi et al., 2023) and are considered to have occurred in historical times.

Therefore, the soft-sediment deformations observed within the predominantly sandy-silt sediments in PSCSA can be interpreted as semites, likely related to the occurrence of seismic events that affected the region in historical times, considering the age of the stratigraphic units that underwent liquefaction.

Conversely, the current liquefaction hazard in PSCSA is considered absent. Although unit 2b exhibits a grain size favorable for liquefaction and Chiaradonna et al. (2024) indicate potential liquefaction, it would not occur due to the absence of very shallow groundwater in boreholes S1 and S2. More specifically, in the Autumn 2020, the water table in boreholes S1 and S2 was encountered at a depth of just over 20 m below ground level. This depth likely represents the shallowest water table level, as the boreholes were drilled in the Autumn which corresponds to the rainy season in Italy. According to the Italian seismic microzonation guidelines (SM Working Group MS (2008), a depth of 20 m is considered the threshold beyond which liquefaction does not occur in sandy deposits. Consequently, in the updated seismic microzonation maps (Tallini et al., 2024) for PSCSA, the liquefaction-prone zone has been removed using the recently acquired water table depth data from boreholes S1 and S2. This pivotal information was unavailable when the map in Figure 2 was created. The absence of liquefaction in PSCSA during the near source 2009 Mw 6.3 L'Aquila earthquake further supports the hypothesis of a negligible liquefaction hazard for PSCSA (Martelli et al., 2012).

5.3 Chronology of the earthquake-induced paleoliquefaction events

The analysis of the western wall of Trench 2 (Figures 6, 7) allowed us to identify at least two earthquake-induced paleoliquefaction events. The methodological approach used to date the paleoliquefaction events was supported by the fact that the pottery shards and charcoal samples were sedimented in alluvial bodies, therefore their age is later (although the exact time difference is unknown) than that of the pottery shards and charcoal samples.

The remarkable mushroom structures, located within unit 5, may be cut by the bottom boundary of unit 2b (Figure 10B), suggesting that unit 5 was involved by a paleoliquefaction event. Its terminus post quem is after the date of charcoal sample found in unit 5 (1,507–1,407 cal BC, SASSA_CARB_5). However, the geometry of the unit 5 and 2b boundary is not very sharp. Therefore, since the relationship between the seismites of unit 5 (Figure 10B) and those of unit 2b is not clear, it cannot be ruled out that the former were generated with the most recent event (PALI2) described below.

The paleoliquefaction event PALI2 occurred after the deposition of unit 4 and prior to the deposition of unit 3 by observing the seismites (deformed varved laminations) in the sands of unit 4 which are cross cut by the erosional surface that separates unit 4 from unit 3 (Figure 10E). These seismites indicate the occurrence of an earthquake immediately following the sedimentation of the sands, which were still well saturated (Moretti and Sabato, 2007).

Radiocarbon dating on charcoal collected within Unit 3 (SASSA_CARB_4: 236–385 cal AD in Supplementary Table 2) and the age of pottery fragments in unit 4 (B in Supplementary Table 1) constrain the age of PALI2 within an interval between 3rd-2nd century BC and the deposition of unit 3 occurring after 236–385 cal AD.

The younger paleoliquefaction event PALI1 occurred after the deposition of unit 3 and before unit 2a. In fact, unit 2b, which is intervening in between unit 3 and 2a, is characterized by soft-sediment deformations such as deformed layers and water escape structures, which suggest the occurrence of a seismic event immediately after the deposition of unit 2b. Further, pseudonodules of unit 3 sediment are mixed within unit 2b sediment which testifies to the involvement of both units in the same paleoliquefaction event (PALI1) (Figure 10D). The water escape structures are represented by sandy dikes which cut vertically through the previous seismites up to the erosion surface. This erosion surface separates unit 2a from 2b, truncating the uppermost portion of the sandy dikes and not allowing the preservation of the sandy volcanos (Figures 7, 10A).

It is worth noting that the relationship between the sandy dikes and the deformed layers does not suggest the occurrence of another seismically induced paleoliquefaction event. In fact, the formation of sandy dikes is a direct consequence of the liquefaction and fluidization of water-saturated sands confined within low-permeability deposits (Audemard and De Santis, 1991; Rodriguez-Pascua et al., 2000; Moretti and Sabato, 2007).

In chronological terms, the age of PALI1 can be inferred from the constraints obtained for unit 3 deposition, which provides a terminus post quem for this event. Specifically, the radiocarbon dating of the charcoal sample (236–385 cal AD) and the age of ceramic material (D in Supplementary Table 1; Supplementary Figure 2; 2nd century AD) suggest PALI1 occurred after the 236–385 cal AD. However, the absence of dating from unit 2a and for the more recent units precludes the establishment of a terminus ad quem or ante quem for PALI1.

5.4 Inferences about earthquake-induced paleoliquefaction events

The paleoseismological investigations allowed us to identify the traces of at least two earthquake-induced paleoliquefaction events. These traces are represented by seismites that affected the stratigraphic sequence, especially in Trench 2, up to unit 2a. These seismites testify to the occurrence of at least two seismic events that impacted the L'Aquila basin during historical times. To clarify which paleoseismic events may have triggered the seismites in PSCSA, several considerations can be made.

According to Rodriguez-Pascua et al. (2000), the seismites of the type here recognized can be attributed to earthquakes of magnitude greater than 6–6.5. The magnitude/epicentral distance relationship proposed by Galli (2000) shows that the liquefaction phenomena in Italy for earthquakes of magnitude greater than 6–6.5 can be triggered at epicentral distances of 45–65 km.

Calculating an average epicentral distance of about 60 km from PSCSA, it is observed that some active faults of the central Apennines (e.g., Galadini and Galli, 2000; Boncio et al., 2004; Falcucci et al., 2016; Galadini et al., 2018), fall within this distance (Figure 1). These active faults have been investigated from a paleoseismological point of view by several Authors, highlighting the occurrence of several surface faulting events during Holocene and in historical times (Galli et al., 2008). In this regard, the analysis of paleoseismological data was carried out to outline the possible paleoearthquakes that may have triggered the seismically induced paleoliquefactions events recognized in PSCSA. Particular attention was paid to those faults whose paleoseismological evidence shows events of activation during a time span consistent with the age of seismites, such as those that occurred in the Roman period (Figure 1). In Table 1 the historical earthquakes associated with the active faults of Central Apennines considered in this study are reported.

Paleoseismological evidence on the Upper Aterno Valley–Paganica fault system (UAVPF) indicates a surface faulting event compatible with the 2 February 1703 historical earthquake on the Mt. Marine fault, the Paganica fault and tentatively also attributed to the Mt. Pettino fault (Moro et al., 2002; 2013; Galli et al., 2011; Cinti et al., 2011). An earlier event was recognised on the Paganica fault and was tentatively attributed by Galli et al. (2011) and Cinti et al. (2011) to the 801 AD seismic event, which struck the central Apennines and Rome (Rovida et al., 2022). However, Moro et al. (2013) provided more precise chronological constraints for this earthquake, suggesting a possible occurrence between the 4th and 6th centuries AD. This conclusion is also supported by archaeoseismological evidence indicating the destruction of the ancient Roman town of Amiternum (northwest of L'Aquila).

Regarding the Middle Aterno Valley–Subequana fault system (MAVSVF), paleoseismological investigations and archaeoseismological data indicate that this fault system ruptured completely during the 2nd-1st century BC (Falcucci et al., 2011; Falcucci et al., 2015).

Paleoseismological and archaeoseismological indications for the Mt. Morrone fault (MF) highlight an activation event in the 2nd century AD (Ceccaroni et al., 2009; Galli et al., 2014).

Regarding the Norcia fault system (NF), paleoseismological investigations performed by Galli et al. (2005) and Galli et al. (2018) indicate that this fault system was responsible for the 14 January 1703 (Mw 7.0) historical earthquake (Rovida et al., 2022) and likely also for an earlier event that occurred in 99 BC.

Paleoseismological indications for the Mt. Vettore-Mt.Bove fault system (MVBF) suggest the activation of the whole structure probably in the 443 AD, an event that caused damages even to Colosseum in Rome (Galli et al., 2019).

Recent paleoseismological investigations suggested that the Assergi-Campo Imperatore fault system (ACIF) caused one of the strongest earthquakes of the 1349 AD seismic sequence (Galli et al., 2022; Gori et al., 2015).

Finally, the Fucino–Mt. Magnola fault system (FMF) is known to be the seismogenic source of the 13 January 1915 historical earthquake. Paleoseismological and archaeoseismological data acquired along this fault indicate that it was responsible for an earlier

TABLE 1 Review of literature data concerning the paleoseismological evidence of the active faults of Central Apennines considered in this study.

Active faults								
		UAVPF	*MAVSVF*	*MF*	*ACIF*	*NF*	*MVBF*	*FMF*
References	Falcucci et al. (2015)		**2nd-1st century BC: PALI2**					
	Falcucci et al. (2011)		2nd-1st century BC: PALI2					
	Galli et al. (2014)			2nd century AD				
	Ceccaroni et al. (2009)			2nd century AD				
	Galli et al. (2019)						443 AD	
	Moro et al. (2013)	**2 February 1703 4th-6th century AD: PALI1**						
	Galli et al. (2022)				1349 AD			
	Cinti et al. (2011)	2 February 1703 801 AD (?)						
	Galli et al. (2011)	2 February 1703 801 AD (?)						
	Galli et al. (2005)					14 January 1703 99 BC		
	Galli et al. (2018)					14 January 1703 99 BC		
	Galadini and Galli (1999)							13 January1915 508 AD (?)

In bold, the earthquakes possibly accountable to the younger (PALI1) and older (PALI2) paleoliquefaction event. UAVPF, Upper Aterno Valley–Paganica fault system; MAVSVF, Middle Aterno Valley–Subequana fault system; MF, Mt. Morrone fault; ACIF, Assergi-Campo Imperatore fault system; NF, Norcia fault system; MVBF, Mt.Vettore-Mt.Bove fault system; FMF, Fucino–Mt. Magnola fault system.

event tentatively attributed to 508 AD (Galadini and Galli, 1999; Galli et al., 2012; Galadini et al., 2022).

Several hypotheses can be made from data reported in Table 1. Regarding the paleoliquefaction event PALI2, which occurred between the 3rd-2nd century BC and 236-385 cal AD (SASSA_CARB_4), it could have been triggered by: (i) the 2nd-1st century BC event of the Middle Aterno Valley-Subequana Valley fault system (MAVSVF), (ii) the 99 BC event of the Norcia fault system (NF) (99 BC) and (iii) the 2nd century AD earthquake originating from the Mt. Morrone fault (MF). Clearly, as the age of the pottery shards represents a post quem for the liquefaction occurrence, the age of deposition of unit 4 is unknown. Consequently, the seismic event cannot be determined with confidence. Anyway, considering the distance of the mentioned faults from PSCSA, it is more likely that the paleoliquefaction event PALI2 may have been triggered by the 2nd-1st century BC event of the Middle Aterno Valley-Subequana Valley fault system (MAVSVF) (Table 2).

Regarding the younger paleoliquefaction event (PALI1), the chronological constraints derived from the charcoal and pottery fragments in unit 3 suggest that this event occurred after 236–385 cal AD (SASSA_CARB_4). Based on the collected references, the younger paleoliquefaction event could have been triggered by: (i) the events of the Upper Aterno Valley-Paganica fault system (UAVPF) (4th-6th century AD and 2 February 1703), (ii) the 14 January 1703 event of the Norcia fault system (NF), (iii) the 443 AD event of the Mt.Vettore-Mt.Bove fault system (MVBF), (iv) the 1349 AD event of the Assergi-Campo Imperatore fault system (ACIF) or (iv) the events of the Fucino-Mt. Magnola fault system (FMF) (508 AD and 13 January 1915). In this case, considering (i) the proximity to PSCSA, (ii) chronological compatibility and (iii) the fact that the liquefied units are currently located several meters above the present alluvial plain, ruling out a very recent age (the last few centuries), it is possible to hypothesize that PALI1 may have been likely triggered by the 4th-6th century AD event of the Upper Aterno Valley- Paganica fault system (UAVPF). Table 2 illustrates the two recognised paleoliquefaction events (PALI1, PALI2), their dating, the units in which the associated seismites were found in the trenches, the causative fault and the related seismic events.

TABLE 2 The two recognised paleoliquefaction events (PALI1, PALI2), their dating, the units in which the associated seismites were found in the trenches, the causative fault and the related seismic events; UAVPF, Upper Aterno Valley–Paganica fault system; MVBF, Mt.Vettore-Mt.Bove fault system; FMF, Fucino–Mt. Magnola fault system; ACIF, Assergi-Campo Imperatore fault system; NF, Norcia fault system; UAVPF, Upper Aterno Valley–Paganica fault system; MAVSVF, Middle Aterno Valley–Subequana fault system; MF, Mt. Morrone fault. (*) the UAVPF and MAVSVF refer to the fault systems accountable for the PALI1 and PALI2, respectively.

PALI	PALI time	Unit	Causative fault	Causative seismic event
PALI1	No data for unit 2b but for sure *ante quem*: ? *post quem*: 236–385 cal AD (SASSA_CARB_4)	2b	**UAVPF(*)** MVBF FMF ACIF NF UAVPF FMF	**4th-6th century AD** 443 AD 508 AD 1349 AD 14 January 1703 AD 2 February 1703 AD 13 January 1915 AD
PALI1	*ante quem*: ? *post quem*: 236–385 cal AD (SASSA_CARB_4)	3	**UAVPF(*)** MVBF FMF ACIF NF UAVPF FMF	**4th-6th century AD** 443 AD 508 AD 1349 AD 14 January 1703 AD 2 February 1703 AD 13 January 1915 AD
PALI2	*ante quem*: 236–385 cal AD (SASSA_CARB_4) *post quem*: possibly post 3rd-2nd cen. BC (pottery shard B)	4	**MAVSVF(*)** NF MF	**2nd-1st century BC** 99 BC 2nd century AD

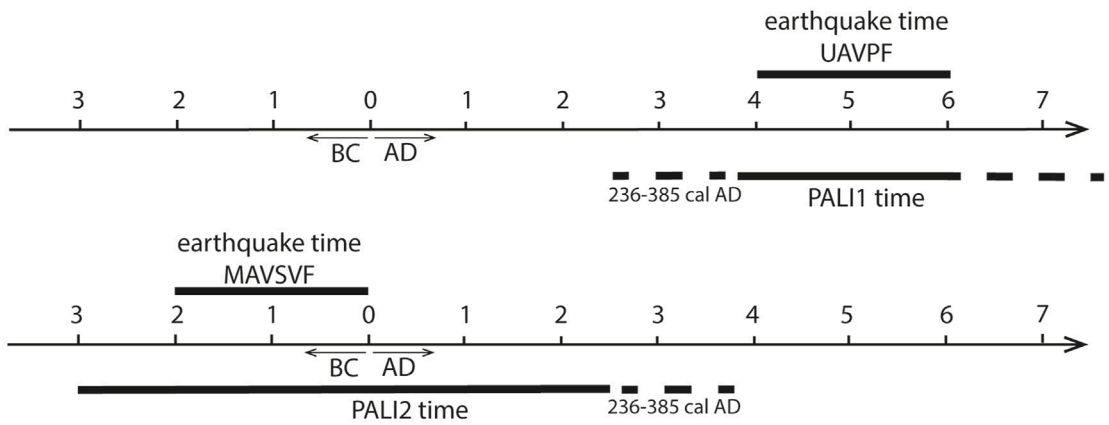

FIGURE 13
The timing of the two recognised paleoliquefaction events (PALI1, PALI2) which were compared to the timing of the probable causative earthquake and fault; UAVPF: Upper Aterno Valley–Paganica fault system; MAVSVF: Middle Aterno Valley–Subequana fault system.

In Figure 13, the timing of the two recognised paleoliquefaction events (PALI1, PALI2) compared to the timing of the probable causative earthquake and fault are reported.

Lastly, another result concerning the paeloliquefactions studied in this work is that they are not reported in the official Italian databases of earthquake-induced ground effects (CEDIT (https://gdb.ceri.uniroma1.it/index.php/view/map/?repository=cedit&project=Cedit) and CFTI-landslides (https://cfti.ingv.it/landslides/).

6 Conclusion

Several geological, geophysical and paleoseismological investigations were carried out to verify the presence and recent activity of the Pagliare di Sassa fault (PSF), which affects PSCSA in which a school building has been planned to be built. Therefore, a study to estimate the geological hazards at the local scale was carried out. Specifically, two paleoseismological trenches (T1 and T2), two continuous boreholes (S1 and S2) and two electrical resistivity tomography (ERT 1 and ERT2) were performed (Figures 3–6, 9).

The analysis of the paleoseismological trenches showed no evidence of faulting due to PSF over the entire exposed stratigraphic sequence, which was dated as more recent than 25 kyr via 14C method. Moreover, the stratigraphic correlation of the units encountered in the boreholes and the lack of morphotectonic scarplets allowed the extension backwards in time the absence in PSCSA of fault dislocation since the Early Pleistocene, which was

also confirmed by the continuous pattern of shallow resistivity layers shown by the two ERT profiles.

Furthermore, paleoseismological trenches instead revealed several soft-sediment deformation structures interpreted as seismites. These seismites are presumably related to the occurrence of large magnitude earthquakes that struck the L'Aquila basin in historical times.

Two earthquake-induced paleoliquefaction events were detected through the dating of carbon samples and pottery fragments. The penultimate event (PALI2) was likely triggered by an earthquake originating from the Middle Aterno Valley-Subequana Valley fault system. This fault system has been paleoseismologically constrained to the 2nd-1st century BC (Falcucci et al., 2011; Falcucci et al., 2015). The last event (PALI1) was likely triggered by an earthquake originating from the Upper Aterno Valley-Paganica fault system. This fault system has been paleoseismologically constrained to the 4th-6th century AD (Moro et al., 2013) (Table 2; Figure 13).

The present study hence demonstrates that assessing fault activity or inactivity needs a comprehensive approach aimed at obtaining a long-time history of the geological evolution of a sector affected by a supposedly active and capable fault, especially in tectonically active regions where it might be easier "to give into the temptation" to deem active a given fault only because it is geometrically and kinematically coherent with the ongoing stress field of the region.

Besides, the seismites identified in PSCSA, provide with useful information to get a better comprehension of the paleoseismic history of the studied area. Indeed, they represent relevant "off-fault" data that support the definition of the chronology of past earthquakes, their possible magnitudes and causative seismogenic source.

In this perspective, most of the information on regional seismotectonics derives from historical seismology and direct "on fault" geological evidence of fault activation. But both these pieces of evidence can be incomplete or affected by a relevant degree of uncertainty. The achievement of data on such seismically induced processes can therefore increase the geological indirect record of seismic shaking and the time of occurrence of past seismic events, hence improving the knowledge on the seismotectonic setting of such a seismically active region as central Italy.

The potential coseismic instabilities at the studied site (PSCSA) were hypothesized to be the PSF surface faulting and liquefactions. This study excluded PSF could be active and capable of surface faulting. The historical paleoliquefactions found in recent colluvium and alluvium (units 5, 4, 3 and 2b) and the grain sorting of unit 2b, favorable to the formation of liquefaction, suggest the potential for this phenomenon. However, since no very shallow groundwater was found in the boreholes S1 and S2, this suggests that liquefaction may not occur at PSCSA due to the lack of very shallow water table. Therefore, both surface faulting and liquefaction hazards should be considered absent at PSCSA. Consequently, PSCSA would be suitable for the construction of the school building.

Lastly, this case study demonstrates that the evaluation of these local seismically induced ground instabilities is a crucial prerequisite for optimal practical considerations regarding land and urban planning, as well as building and infrastructure design, particularly for significant structures like school buildings, as exemplified by the Pagliare di Sassa case study site.

Data availability statement

The raw data supporting the conclusions of this article will be made available by the authors, without undue reservation.

Author contributions

MT: Writing–original draft, Writing–review and editing. DM: Writing–original draft, Writing–review and editing. EF: Writing–original draft, Writing–review and editing. FG: Writing–original draft, Writing–review and editing. SG: Writing–original draft, Writing–review and editing. VG: Writing–original draft, Writing–review and editing. MaS: Writing–original draft, Writing–review and editing. MM: Writing–original draft, Writing–review and editing. MiS: Writing–original draft, Writing–review and editing.

Funding

The author(s) declare that financial support was received for the research and/or publication of this article. This study is part of the 3rd level seismic microzonation project activities carried out on pilot areas located in the L'Aquila Municipality area. Therefore, we would like to thank (i) the Abruzzo Region (Department of Government of the Territory and Environmental Policies–Risk Prevention Service of Civil Protection, and (ii) L'Aquila Municipality for funding the aforementioned project and the *in-situ* investigations at the Pagliare di Sassa case study site, respectively (CUP: C17B15002250001; CUP: C15C18000120001). The research leading to these results has also received funding from the Italian Ministry of Economic Development (MiSE) under the project "SICURA—CASA INTELLIGENTE DELLE TECNOLOGIE PER LA SICUREZZA," Grant Id: C19C20000520004. Moreover, the research described in this contribution has been partially developed in the framework of the research project National Centre for HPC, Big Data and Quantum Computing - PNRR Project, funded by the European Union - Next-Generation EU.

Acknowledgments

We would also like to thank warmly Stefano Brusaporci and Pamela Maiezza for the laser scan acquisition and processing and the photogrammetric survey of the two trenches.

Conflict of interest

The authors declare that the research was conducted in the absence of any commercial or financial relationships that could be construed as a potential conflict of interest.

The author(s) declared that they were an editorial board member of Frontiers, at the time of submission. This had no impact on the peer review process and the final decision.

Generative AI statement

The author(s) declare that no Generative AI was used in the creation of this manuscript.

Publisher's note

All claims expressed in this article are solely those of the authors and do not necessarily represent those of their affiliated organizations, or those of the publisher, the editors and the reviewers. Any product that may be evaluated in this article, or claim that may be made by its manufacturer, is not guaranteed or endorsed by the publisher.

Supplementary material

The Supplementary Material for this article can be found online at: https://www.frontiersin.org/articles/10.3389/feart.2025.1523730/full#supplementary-material

References

Antonielli, B., Della Seta, M., Esposito, C., Mugnozza, G. S., Schilirò, L., Spadi, M., et al. (2020). Quaternary rock avalanches in the Apennines: new data and interpretation of the huge clastic deposit of the L'Aquila Basin (central Italy). *Geomorphology* 361, 107194. doi:10.1016/j.geomorph.2020.107194

Audemard, F. A., and De Santis, F. (1991). Survey of liquefaction structures induced by recent moderate earthquakes. *Bullettin Int. Assoc. Eng. Geol.* 44 (1), 5–16. doi:10.1007/bf02602705

Barchi, M., Galadini, F., Lavecchia, G., Messina, P., Michetti, A. M., Peruzza, L., et al. (2000). *Sintesi delle conoscenze sulle faglie attive in Italia Centrale: parametrizzazione ai fini della caratterizzazione della pericolosità sismica [Summary of knowledge on active faults in Central Italy: parameterization for the purposes of characterizing seismic hazard]*. Roma: CNR Gruppo Nazionale per la Difesa dai Terremoti, 62.

Basi, M., Boncio, P., Milana, G., Piacentini, T., Pipponzi, G., Pizzi, A., et al. (2012). Standard di rappresentazione cartografica e archiviazione informatica - specifiche tecniche per la redazione degli elaborati cartografici ed informatici relativi al primo livello delle attività di Microzonazione sismica (ver. 1.2) [Standard of mapping and Informatic archiving relating to the first level of seismic microzonation activities]. *Gruppo Lav. attività Microzonazione sismica, Reg. Abruzzo*. Available online at: https://protezionecivile.regione.abruzzo.it/agenzia/files/rischio%20sismico/microzonazione/OPCM3907/LineeGuidaMS_v1_2_ONLINE2.pdf (Accessed March 27, 2025).

Blumetti, A. M. (1995). Neotectonic investigations and evidence of paleoseismicity in the epicentral area of the January–February 1703, Central Italy, earthquakes. *Perspect. paleoseismology* 6, 83–100.

Boncio, P., Amoroso, S., Galadini, F., Galderisi, A., Iezzi, G., and Liberi, F. (2020). Earthquake-induced liquefaction features in a late Quaternary fine-grained lacustrine succession (Fucino Lake, Italy): implications for microzonation studies. *Eng. Geol.* 272 (2020), 105621. doi:10.1016/j.enggeo.2020.105621

Boncio, P., Amoroso, S., Vessia, G., Francescone, M., Nardone, M., Monaco, P., et al. (2018). Evaluation of liquefaction potential in an intermountain Quaternary lacustrine basin (Fucino basin, central Italy). *Bull. Earthq. Eng.* 16, 91–111. doi:10.1007/s10518-017-0201-z

Boncio, P., Galli, P., Naso, G., and Pizzi, A. (2012). Zoning surface rupture hazard along normal faults: insight from the 2009 M w 6.3 L'Aquila, Central Italy, earthquake and other global earthquakes. *Bull. Seismol. Soc. Am.* 102 (3), 918–935. doi:10.1785/0120100301

Boncio, P., Lavecchia, G., and Pace, B. (2004). Defining a model of 3D seismogenic sources for seismic hazard assessment applications: the case of central Apennines (Italy). *J. Seismol.* 8 (3), 407–425. doi:10.1023/B:JOSE.0000038449.78801.05

Boncio, P., Pizzi, A., Brozzetti, F., Pomposo, G., Lavecchia, G., Di Naccio, D., et al. (2010). Coseismic ground deformation of the 6 april 2009. L'Aquila earthquake (central Italy, Mw6.3). *Geophys Res. Lett.* 37, L06308. doi:10.1029/2010GL042807

Boulanger, R. W., and Idriss, I. M. (2014). *CPT and SPT based liquefaction triggering procedure. Report No. UCD/CGM-14/01, center for geotechnical modelling, department of Civil and enviromentally engineering*. California: Univ. California, 134. doi:10.1061/(ASCE)GT.1973-5606.0001388

Carminati, E., Lustrino, M., Cuffaro, M., and Doglioni, C. (2010). Tectonics, magmatism and geodynamics of Italy: what we know and what we imagine. In: (Eds.) M. Beltrando, A. Peccerillo, M. Mattei, S. Conticelli, and C. Doglioni *The Geology of Italy: tectonics and life along plate margins, Journal of the Virtual Explorer*. doi:10.3809/jvirtex.2010.00226

Cavinato, G. P., and De Celles, P. G. (1999). Extensional basins in the tectonically bimodal central Apennines fold-thrust belt, Italy: response to corner flow above a subducting slab in retrograde motion. *Geology* 27, 955–958. doi:10.1130/0091-7613(1999)027<0955:EBITTB>2.3.CO;2

Ceccaroni, E., Ameri, G., Gómez Capera, A. A., and Galadini, F. (2009). The 2nd century AD earthquake in central Italy: archaeoseismological data and seismotectonic implications. *Nat. hazards* 50 (2), 335–359. doi:10.1007/s11069-009-9343-x

Centamore, E., and Dramis, F. (2010). *Note illustrative della Carta geologica d'Italia alla scala 1:50.000, foglio 358-pescorocchiano [illustrative notes of the geological map of Italy at 1:50,000 scale, sheet 358-pescorocchiano]*. ISPRA-Servizio Geologico d'Italia, Ente realizzatore Regione Lazio, 147. Available online at: http://www.isprambiente.gov.it/Media/carg/note_illustrative/358_Pescorocchiano.pdf (Accessed February 24, 2024).

Chiaradonna, A., Monaco, P., and Tallini, M. (2024). "Investigations and liquefaction assessment at the Pagliare di Sassa site (L'Aquila, Central Italy)," in *Proceedings of 18th world conference on earthquake engineering* (Milan).

Chiaradonna, A., Spadi, M., Monaco, P., Papasodaro, F., and Tallini, M. (2021). Seismic soil characterization to estimate site effects induced by near-fault earthquakes: the case study of pizzoli (Central Italy) during the Mw 6.7 2 february 1703, earthquake. *Geosciences* 12 (1), 2. doi:10.3390/geosciences12010002

Chiaraluce, L. (2012). Unravelling the complexity of Apenninic extensional fault systems: a review of the 2009 L'Aquila earthquake (Central Apennines, Italy). *J. Struct. Geol.* 42, 2–18. doi:10.1016/j.jsg.2012.06.007

Cinti, F. R., Pantosti, D., De Martini, P. M., Pucci, S., Civico, R., Pierdominici, S., et al. (2011). Evidence for surface faulting events along the Paganica fault prior to the 6 April 2009 L'Aquila earthquake (central Italy). *J. Geophys Res.* 116, B07308. doi:10.1029/2010JB007988

Commissione tecnica per la microzonazione sismica (2015). *Linee guida per la gestione del territorio in aree interessate da Faglie Attive e Capaci (FAC), versione 1.0 [Guidelines for land management in areas affected by Active and Capable Faults (FAC), version 1.0]*. Roma: Conferenza delle Regioni e delle Province Autonome – Dipartimento della protezione civile.

Cosentino, D., Asti, R., Nocentini, M., Gliozzi, E., Kotsakis, T., Mattei, M., et al. (2017). New insights into the onset and evolution of the central Apennine extensional intermontane basins based on the tectonically active L'Aquila Basin (central Italy). *Bull. Geol. Soc. Am.* 129, 1314–1336. doi:10.1130/B31679.1

Cosentino, D., Cipollari, P., Marsili, P., and Scrocca, D. (2010). Geology of the central Apennines: a regional review. *J. Virtual Explor* 36. doi:10.3809/jvirtex.2010.00223

De Martini, P. M., Cinti, F. R., Cucci, L., Smedile, A., Pinzi, S., Brunori, C. A., et al. (2012). Sand volcanoes induced by the April 6th 2009 Mw 6.3 L'Aquila earthquake: a case study from the Fossa area. *Italian J. Geosciences* 131 (3), 410–422. doi:10.3301/IJG.2012.14

Devoti, R., Pietrantonio, G., Pisani, A., Riguzzi, F., and Serpelloni, E. (2010). Present day kinematics of Italy. In: (Eds.) M. Beltrando, A. Peccerillo, M. Mattei, and S. Conticelli, *The Geology of Italy: tectonics and life along plate margins*, Journal of the Virtual Explorer, 36, 2. doi:10.3809/jvirtex.2010.0023

Diss Working Group (2018). Database of Individual Seismogenic Sources (DISS), Version 3.2.1: a compilation of potential sources for earthquakes larger than M 5.5 in Italy and surrounding areas. Available online at: http://diss.rm.ingv.it/diss/,IstitutoNazionalediGeofisicaeVulcanologia.

Durante, F., Di Giulio, G., Tallini, M., Milana, G., and Macerola, L. (2017). A multidisciplinary approach to the seismic characterization of a mountain

top (Monteluco, central Italy). *Phys. Chem. Earth Parts A/B/C* 98, 119–135. doi:10.1016/j.pce.2016.10.015

Emergeo Working Group (2010). Evidence for surface rupture associated with the Mw 6.3 L'Aquila earthquake sequence of April 2009 (central Italy). *Terra nova.* 22, 43–51. doi:10.1111/j.1365-3121.2009.00915.x

Fäh, D., Rüttener, E., Noack, T., and Kruspan, P. (1997). Microzonation of the city of basel. *J. Seismol.* 1, 87–102. doi:10.1023/a:1009774423900

Falcucci, E., Gori, S., Galadini, F., Fubelli, G., Moro, M., and Saroli, M. (2016). Active faults in the epi-central and mesoseismal Ml 6.0 24, 2016 Amatrice earthquake region, central Italy. Methodological and seismotectonic issues. *Ann. Geophys.* 59 (5), 1–6. doi:10.4401/ag-7266

Falcucci, E., Gori, S., Moro, M., Fubelli, G., Saroli, M., Chiarabba, C., et al. (2015). Deep reaching versus vertically restricted Quaternary normal faults: implications on seismic potential assessment in tectonically active regions: lessons from the middle Aterno valley fault system, central Italy. *Tectonophysics* 651, 186–198. doi:10.1016/j.tecto.2015.03.021

Falcucci, E., Gori, S., Moro, M., Pisani, A. R., Melini, D., Galadini, F., et al. (2011). The 2009 L'Aquila earthquake (Italy): what's next in the region? Hints from stress diffusion analysis and normal fault activity. *Earth Planet. Sci. Lett.* 305 (3-4), 350–358. doi:10.1016/j.epsl.2011.03.016

Falcucci, E., Gori, S., Peronace, E., Fubelli, G., Moro, M., Saroli, M., et al. (2009). The Paganica fault and surface coseismic ruptures caused by the 6 april 2009 earthquake (L'Aquila, Central Italy). *Seismol. Res. Lett.* 80, 940–950. doi:10.1785/gssrl.80.6.940

Galadini, F., Ceccaroni, E., Dixit Dominus, G., Falcucci, E., Gori, S., Maceroni, D., et al. (2022). Combining Earth Sciences with Archaeology to investigate natural risks related to the cultural heritage of the Marsica region (central Apennines, Italy). *Mediterr. Geosci. Rev.* 4, 287–318. doi:10.1007/s42990-022-00078-9

Galadini, F., Falcucci, E., Galli, P., Giaccio, B., Gori, S., Messina, P., et al. (2012). Time intervals to assess active and capable faults for engineering practices in Italy. *Eng. Geol.* 139-140, 50–65. doi:10.1016/j.enggeo.2012.03.012

Galadini, F., Falcucci, E., Gori, S., Zimmaro, P., Cheloni, D., and Stewart, J. P. (2018). Active faulting in source region of 2016–2017 Central Italy event sequence. *Earthq. Spectra* 34 (4), 1557–1583. doi:10.1193/101317EQS204M

Galadini, F., and Galli, P. (1999). The Holocene paleoearthquakes on the 1915 Avezzano earthquake faults (central Italy): implications for active tectonics in the central Apennines. *Tectonophysics* 308, 143–170. doi:10.1016/S0040-1951(99)00091-8

Galadini, F., and Galli, P. (2000). Active tectonics in the central Apennines (Italy) and input data for seismic hazard assessment. *Nat. Haz* 22, 225–270. doi:10.1023/A:1008149531980

Galadini, F., Galli, P., and Moro, M. (2003). Paleoseismology of silent faults in the central Apennines (Italy): the Campo Imperatore fault (gran sasso range fault system). *Ann. Geophys.* 46, 793–813.

Galadini, F., and Messina, P. (1994). Plio-Quaternary tectonics of the Fucino basin and surroundings areas (central Italy). *G. Geol.* 56 (2), 73–99.

Galli, P. (2000). New empirical relationships between magnitude and distance for liquefaction. *Tectonophysics* 324, 169–187. doi:10.1016/S0040-1951(00)00118-9

Galli, P., Galadini, F., and Calzoni, F. (2005). Surface faulting in Norcia (central Italy): a "paleoseismological perspective". *Tectonophysics* 403, 117–130. doi:10.1016/j.tecto.2005.04.003

Galli, P., Galadini, F., Moro, M., and Giraudi, C. (2002). New paleoseismological data from the Gran Sasso d'Italia area (central Apennines). *Geophys. Res. Lett.* 29 (7), 1134. doi:10.1029/2001GL013292

Galli, P., Galadini, F., and Pantosti, D. (2008). Twenty years of paleoseismology in Italy. *Earth-Science Rev.* 88, 89–117. doi:10.1016/j.earscirev.2008.01.001

Galli, P., Galderisi, A., Ilardo, I., Piscitelli, S., Scionti, V., Bellanova, J., et al. (2018). Holocene paleoseismology of the Norcia fault system (Central Italy). *Tectonophysics* 745, 154–169. doi:10.1016/j.tecto.2018.08.008

Galli, P., Galderisi, A., Messina, P., and Peronace, E. (2022). The Gran Sasso fault system: paleoseismological constraints on the catastrophic 1349 earthquake in Central Italy. *Tectonophysics* 822, 229156. doi:10.1016/j.tecto.2021.229156

Galli, P., Galderisi, A., Peronace, E., Giaccio, B., Hajdas, I., Messina, P., et al. (2019). The awakening of the dormant mount vettore fault (2016 Central Italy earthquake, M_w 6.6): paleoseismic clues on its millennial silences. *Tectonics* 38 (2), 687–705. doi:10.1029/2018TC005326

Galli, P., Giaccio, B., and Messina, P. (2010). The 2009 central Italy earthquake seen through 0.5 Myr-long tectonic history of the L'Aquila faults system. *Quat. Sci. Rev.* 29, 3768–3789. doi:10.1016/j.quascirev.2010.08.018

Galli, P., Giaccio, B., Peronace, E., and Messina, P. (2014). Holocene paleoearthquakes and early–late Pleistocene slip rate on the sulmona fault (central apeninnes, Italy). *Bull. Seismol. Soc. Am.* 105 (1), 1–13. doi:10.1785/0120140029

Galli, P., Messina, P., Giaccio, B., Peronace, E., and Quadrio, B. (2012). Early Pleistocene to late Holocene activity of the Magnolia fault (Fucino fault system, central Italy). *Boll. Geofis. Teor. Appl.* 53 (4). doi:10.4430/bgta0054

Galli, P. A. C., Giaccio, B., Messina, P., Peronace, E., and Zuppi, G. M. (2011). Palaeoseismology of the L'Aquila faults (central Italy, 2009, Mw 6.3 earthquake): implications for active fault linkage. *Geophys J. Int.* 187, 1119–1134. doi:10.1111/j.1365-246X.2011.05233.x

Gazetas, G., Pecker, A., Faccioli, E., Paolucci, R., and Anastasopoulos, I. (2008). Preliminary design recommendations for dip–slip fault–foundation interaction. *Bull. Earthq. Eng.* 6, 677–687. doi:10.1007/s10518-008-9082-5

Giallini, S., Sirianni, P., Pagliaroli, A., Pizzi, A., Mancini, M., Kaiser, A., et al. (2024). Reconstruction of a subsoil model for local seismic response evaluation through experimental and numerical methods: the case of the Wellington CBD, New Zealand. *Eng. Geol.* 330, 107413. doi:10.1016/j.enggeo.2024.107413

Gori, S., Falcucci, E., Atzori, S., Chini, M., Moro, M., Serpelloni, E., et al. (2012). Constraining primary surface rupture length along the Paganica fault (2009 L'Aquila earthquake) with geological and geodetic (DInSAR and GPS) data. *Ital. J. Geosci.* 131, 359–372. doi:10.3301/IJG.2012.21

Gori, S., Falcucci, E., Dramis, F., Galadini, F., Galli, P., Giaccio, B., et al. (2014). Deep-seated gravitational slope deformation, large-scale rock failure, and active normal faulting along Mt. Morrone (Sulmona basin, Central Italy): geomorphological and paleoseismological analyses. *Geomorphology* 208, 88–101. doi:10.1016/j.geomorph.2013.11.017

Gori, S., Falcucci, E., Moro, M., Saroli, M., Fubelli, G., Chiarabba, C., et al. (2015). Recent advances in the comprehension of the central Apennine seismotectonics, by cross-checking Quaternary geology, paleoseismological and seismological data. *6th Int. INQUA Meet. Paleoseismology, Act. Tect. Archaeoseismology* 19, 24.

Guerrieri, L., Blumetti, A. M., Di Manna, P., Serva, L., and Vittori, E. (2009). The exposure of urban areas to surface faulting hazard in Italy; a quantitative analysis. *Italian J. Geosciences (Bollettino della Soc. Geol. Italiana)* 128, 179–189.

Herrmann, R. B., Malagnini, L., and Munafò, I. (2011). *Regional moment tensors of the 2009 L'Aquila earthquake*.

Idriss, I. M., and Boulanger, R. W. (2008). *Soil liquefaction during earthquakes*. Earthquake Engineering Research Institute, Oakland, CA, 237 p.p.

Iezzi, F., Boncio, P., Testa, A., Di Giulio, G., Vassallo, M., Cara, F., et al. (2023). A case study of multidisciplinary surface faulting assessment in the urbanized Fucino basin, Italy. *Italian J. Geosciences* 142 (1), 104–121. doi:10.3301/IJG.2023.03

ISPRA (2010). Geological map of Italy at 1:50,000 scale, sheet n° 358 Pescorocchiano. *Ist. Poligr. dello Stato*. Available online at: https://www.isprambiente.gov.it/Media/carg/358_PESCOROCCHIANO/Foglio.html (Accessed March 27, 2025).

ITHACA Working Group (2019). "ITHACA (ITalyHAzard from CApable faulting), A database of active capable faults of the Italian territory," in *Version december 2021* (ISPRA Geological Survey of Italy. Web Portal). Available online at: http://sgi2.isprambiente.it/ithacaweb/Mappatura.aspx.

Lavecchia, G., Ferrarini, F., Brozzetti, F., De Nardis, R., Boncio, P., and Chiaraluce, L. (2012). From surface geology to aftershock analysis: constraints on the geometry of the L'Aquila 2009 seismogenic fault system. *Ital. J. Geosci. Boll. Soc. Geol. It* 131 (3), 330–347. doi:10.3301/IJG.2012.24

Maceroni, D., Dixit, D. G., Gori, S., Falcucci, E., Galadini, F., Moro, M., et al. (2022). First evidence of the late Pleistocene – Holocene activity of the Roveto Valley fault (central Apennines, Italy). *Front. Earth Sci.* 10, 1018737. doi:10.3389/feart.2022.1018737

Mancini, M., Cavuoto, G., Pandolfi, L., Petronio, C., Salari, L., and Sardella, R. (2012). Coupling basin infill history and mammal biochronology in a Pleistocene intramontane basin: the case of western L'Aquila Basin (central Apennines, Italy). *Quat. Int.* 267, 62–77. doi:10.1016/j.quaint.2011.03.020

Martelli, L., Boncio, P., Baglione, M., Cavuoto, G., Mancini, M., Mugnozza, G. S., et al. (2012). Main geologic factors controlling site response during the 2009 L'Aquila earthquake. *Italian J. Geosciences* 131 (3), 423–439. doi:10.3301/IJG.2012.12

McCalpin, J. (2009). *Paleoseismology*. Second edition. Burlington, San Diego, London: Academic Press, 629.

Michetti, A. M., Brunamonte, F., Serva, L., and Whitney, R. A. (1995). Seismic hazard assessment from paleoseismological evidence in the Rieti Region (Central Italy). *Perspect. Paleoseismology", Assoc. Eng. Geol. Bull. Special Publ.* (6), 63–82.

Molnar, S., Assaf, J., Sirohey, A., and Adhikari, S. R. (2020). Overview of local site effects and seismic microzonation mapping in Metropolitan Vancouver, British Columbia, Canada. *Eng. Geol.* 270, 105568. doi:10.1016/j.enggeo.2020.105568

Monaco, P., De Magistris, F. S., Grasso, S., Marchetti, S., Maugeri, M., and Totani, G. (2011). Analysis of the liquefaction phenomena in the village of Vittorito (L'Aquila). *Bull. Earthq. Eng.* 9 (1), 231–261. doi:10.1007/s10518-010-9228-0

Moretti, M., and Sabato, L. (2007). Recognition of trigger mechanisms for soft-sediment deformation in the Pleistocene lacustrine deposits of the Sant'Arcangelo Basin (Southern Italy): seismic shock vs. overloading. *Sediment. Geol.* 196, 31–45. doi:10.1016/j.sedgeo.2006.05.012

Mori, F., Mendicelli, A., Moscatelli, M., Romagnoli, G., Peronace, E., and Naso, G. (2020). A new Vs30 map for Italy based on the seismic microzonation dataset. *Eng. Geol.* 275, 105745. doi:10.1016/j.enggeo.2020.105745

Moro, M., Bosi, V., Galadini, F., Galli, P., Giaccio, B., Messina, P., et al. (2002). Analisi paleosismologiche lungo la faglia del M. Marine (alta valle dell'Aterno): risultati preliminari. *Alp. Mediterr. Quat.* 15 (2), 259–270. Available online at: https://amq.aiqua.it/index.php/amq/article/view/611.

Moro, M., Falcucci, E., Gori, S., Saroli, M., and Galadini, F. (2016). New paleoseismic data across the Mt. Marine Fault between the 2016 Amatrice and 2009 L'Aquila seismic sequences (central Apennines). *Ann. Geophys. 59 Fast Track* 5 2016. doi:10.4401/ag-7260

Moro, M., Gori, S., Falcucci, E., Saroli, M., Galadini, F., and Salvi, S. (2013). Historical earthquakes and variable kinematic behaviour of the 2009 L'Aquila seismic event (central Italy) causative fault, revealed by paleoseismological investigations. *Tectonophysics* 583, 131–144. doi:10.1016/j.tecto.2012.10.036

Moscatelli, M., Albarello, D., Scarascia Mugnozza, G., and Dolce, M. (2020). The Italian approach to seismic microzonation. *Bull. Earthq. Eng.* 18 (12), 5425–5440. doi:10.1007/s10518-020-00856-6

Nocentini, M., Asti, R., Cosentino, D., Durante, F., Gliozzi, E., Macerola, L., et al. (2017). Plio-quaternary geology of L'Aquila-Scoppito basin (Central Italy). *J. Maps* 13, 563–574. doi:10.1080/17445647.2017.1340910

Obermeier, S. F. (1996). Use of liquefaction-induced features for paleoseismic analysis – an overview of how seismic liquefaction features can be distinguished from other features and how their regional distribution and properties of source sediment can be used to infer the location and strength of Holocene paleo-earthquakes. *Eng. Geol.* 44, 1–76. doi:10.1016/S0013-7952(96)00040-3

Oddone, E. (1915). Gli elementi fisici del grande terremoto marsicano-fucense del 13 gennaio 1915. *Boll. Soc. Sismol. Ital.* 19, 71–215.

Ohsaki, Y. (1972). Japanese microzonation methods. *Bull. Earthq. Res. Inst.* 49, 161–182.

Paolucci, R., Mariani, S., and Griffini, S. (2010). Simplified modelling of continous buried pipelines subject to earthquake fault rupture. *Earthq. Struct.* 1, 253–267. doi:10.12989/eas.2010.1.3.253

Pondrelli, S., Salimbeni, S., Ekstrom, G., Morelli, A., Gasperini, P., and Vannucci, G. (2006). The Italian CMT dataset from 1977 to the present. *Phys. Earth Planet Inter* 159, 286–303. doi:10.1016/j.pepi.2006.07.008

Rodriguez Pasua, M. A., Calvo, J. P., De Vicente, G., and Gomez Gras, D. (2000). Soft-sediment deformation structures interpreted as semites in lacustrine sediments of the Prebetic Zone, SE Spain, and their potential use as indicators of earthquake magnitudes during the Late Miocene. *Sediment. Geol.* 135, 117–135. doi:10.1016/S0037-0738(00)00067-1

Rollins, K. M., Roy, J., Athanasopoulos-Zekkos, A., Zekkos, D., Amoroso, S., and Cao, Z. (2021). A new dynamic cone penetration test-based procedure for liquefaction triggering assessment of gravelly soils. *J. Geotech. Geoenviron. Eng.* 147 (12), 04021141. doi:10.1061/(ASCE)GT.1943-5606.0002686

Rovida, A., Locati, M., Camassi, R., Lolli, B., Gasperini, P., and Antonucci, A. (2022). *Catalogo Parametrico dei Terremoti Italiani (CPTI15), versione 4.0 [Parametric Catalog of Italian Earthquakes (CPTI15), version 4.0]*. Istituto Nazionale di Geofisica e Vulcanologia. doi:10.13127/CPTI/CPTI15.4

Salocchi, A. C., Minarelli, L., Lugli, S., Amoroso, S., Rollins, K. M., and Fontana, D. (2020). Liquefaction source layer for sand blows induced by the 2016 megathrust earthquake (MW 7.8) in Ecuador (Boca de Briceno). *J. South Am. Earth Sci.* 103, 102737. doi:10.1016/j.jsames.2020.102737

Salvatore, N., Pizzi, A., Rollins, K. M., Pagliaroli, A., and Amoroso, S. (2022). Liquefaction assessment of gravelly soils: the role of *in situ* and laboratory geotechnical tests through the case study of the Sulmona basin (Central Italy). *Italian J. Geosciences* 141 (2), 216–229. doi:10.3301/IJG.2022.18

Salvi, S., Cinti, F. R., Colini, L., D'Addezio, G., Doumaz, F., and Pettinelli, E. (2003). Investigation of the active Celano–L'Aquila fault system, Abruzzi (central Apennines, Italy) with combined ground-penetrating radar and palaeoseismic trenching. *Geophys. J. Int.* 155 (3), 805–818. doi:10.1111/j.1365-246X.2003.02078.x

Sherif, M. A., Ishibashi, I., and Tsuchiya, C. (1977). Saturation effects on initial soil liquefaction. *J. Geotechnical Eng. Div. ASCE* 103, 914–917. doi:10.1061/ajgeb6.0000477

SM Working Group MS (2008). *Indirizzi e criteri per la microzonazione sismica [Guidelines for Seismic Microzonation]*. Rome: Conference of Regions and Autonomous Provinces of Italy – Civil Protection Department.

Spadi, M., Maceroni, D., Dixit Dominus, G., Tallini, M., Falcucci, E., Galadini, F., et al. (2022). Surface faulting and liquefaction hazard assessment in the central Apennines for land use practices: a case study from the L'Aquila urban area (central Italy), *EGU General Assem. 2022*. doi:10.5194/egusphere-egu22-6312

Storti, F., Aldega, L., Balsamo, F., Corrado, S., Del Monaco, F., Di Paolo, L., et al. (2013). Evidence for strong middle Pleistocene earthquakes in the epicentral area of the 6 April 2009 L'Aquila seismic event from sediment paleofluidization and overconsolidation. *J. Geophys. Res.* 118 (7), 3767–3784. doi:10.1002/jgrb.50254

Tallini, M., Durante, F., Macerola, L., and Nocentini, M. (2014). Carta di Microzonazione sismica di primo livello, Carta Geologico-tecnica a scala 1:5000, foglio 3, zona Preturo, Comune dell'Aquila, Regione Abruzzo First level seismic microzonation map at scale 1:5000, sheet 3, Preturo zone, L'Aquila Municipality, Abruzzo Region. Available online at: https://protezionecivile.regione.abruzzo.it/agenzia/files/rischio%20sismico/microzonazione/MOPS/AQ_Preturo_Sassa.pdf (Accessed February 24, 2024).

Tallini, M., Morana, E., Guerriero, V., Di Giulio, G., and Vassallo, M. (2024). Seismic microzonation mapping for urban and land sustainable planning in high seismicity areas (L'aquila municipality, Central Italy): the contribution of 2D modeling for the evaluation of the amplification factors. *Sustainability* 16, 8401. doi:10.3390/su16198401

Tallini, M., Spadi, M., Cosentino, D., Nocentini, M., Cavuoto, G., and Di Fiore, V. (2019). High-resolution seismic reflection exploration for evaluating the seismic hazard in a Plio-Quaternary intermontane basin (L'Aquila downtown, central Italy). *Quat. Int.* 532, 34–47. doi:10.1016/j.quaint.2019.09.016

Technical Commission on Seismic Microzonation (2015). *Land use guidelines for areas with active and capable faults (ACF), conference of the Italian regions and autonomous provinces – Civil protection department*. Rome.

Tsuchida, H., and Hayashi, S. (1971). "Estimation of liquefaction potential of sandy soils," in *Proceedings of the 3rd joint meeting, us–Japan panel on wind and seismic effects, may 1971* (Tokyo: UJNR), 91–109.

Valoroso, L., Chiaraluce, L., Piccinini, D., Di Stefano, R., Schaff, D., and Waldhauser, F. (2013). Radiography of a normal fault system by 64,000 high-precision earthquake locations: the 2009 L'Aquila (central Italy) case study. *J. Geophys. Res. Solid Earth* 118, 1156–1176. doi:10.1002/jgrb.50130

Yamazaki, F., and Maruyama, Y. (2020). "Seismic microzonation," in *Encyclopedia of solid earth geophysics. Encyclopedia of earth sciences series*. Editor H. Gupta (Cham: Springer). doi:10.1007/978-3-030-10475-7_187-1